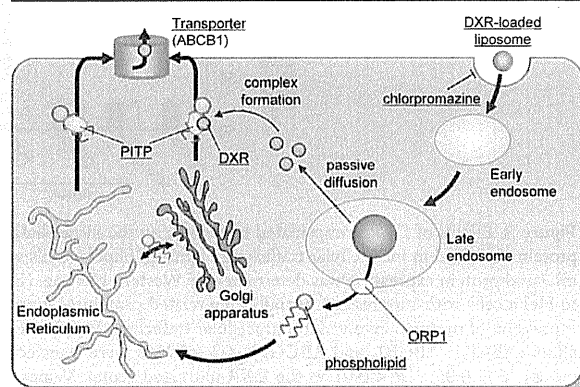


**Figure 4.** Effects of lipid components on intracellular trafficking and cytotoxicity of DXR. (A, B) Intracellular concentrations of DXR encapsulated in PEG-modified liposomes 24 h after adding the liposomes to HeLa cells with suppression of trafficking-related proteins. siRNAs were used to suppress the expression of proteins involved in the intracellular trafficking of phospholipids from the ER/Golgi apparatus to the cell membrane (ORP2 and P1TP) (A) and the extracellular efflux (ABCA1, ABCB1, ABCC1, and ABCG1) (B). \*\* $P < 0.01$  vs the corresponding control group. Values are presented as mean  $\pm$  SD ( $n = 6$ ). (C) Cytotoxicity of DXR encapsulated in PEG-modified liposomes in HeLa cells with suppression of P1TP and ABCB1 expression. Cytotoxicity was evaluated using a WST-8 assay. \*\* $P < 0.01$  vs the corresponding control group lacking DXR; †† $P < 0.01$  vs the corresponding control group. Values are presented as mean  $\pm$  SD ( $n = 6$ ). (D) Evaluation of complexes of P1TP, phospholipids, and DXR. Liposomes generated using NBD-labeled DSPC (1.0  $\mu$ g) and DXR (0.1  $\mu$ g) were mixed with HeLa cell lysates containing P1TP (10  $\mu$ g protein). (E) Intracellular concentrations of DXR at 24 h after adding liposomes to HeLa cells with suppression of ORP2 and P1TP expression. \*\* $P < 0.01$  vs the corresponding control group. Values are presented as mean  $\pm$  SD ( $n = 6$ ).

a substrate of ABCB1.<sup>33–35</sup> However, when cells were treated with DXR encapsulated in PEG-modified liposomes, we found that the intracellular concentrations of DXR were increased by the suppression of ABCB1 and P1TP expression (Figures 4A and 4B). In fact, suppression of ABCB1 and P1TP expression increased the cytotoxicity of DXR encapsulated in PEG-modified liposomes in HeLa cells (Figure 4C). These observations suggest that P1TP is involved in the intracellular trafficking of liposome-encapsulated DXR. Although, several reports have shown that P1TP is involved in the transport of phosphatidylcholine and phosphatidylinositol,<sup>29,36,37</sup> there are

no reports showing that P1TP is involved in DXR transport. Therefore, we evaluated the formation of complexes of P1TP, liposomal phospholipids, and DXR. As shown in Figures 4D and 4E, DXR formed a complex with P1TP in the presence of phospholipids, and the intracellular concentration of DXR increased following suppression of P1TP expression and preincubation with phospholipids. These results indicate that the intracellular trafficking of DXR released from liposomes to the endosome/lysosome is controlled by P1TP, which forms a complex with phospholipids and DXR released from DXR-encapsulated liposomes (Figure 5).



**Figure 5.** Predicted mechanism of the intracellular trafficking of liposome-encapsulated DXR.

It is known that the intracellular trafficking of DXR is controlled by passive diffusion. Therefore, while several studies have focused on the intracellular uptake process of DXR encapsulated into liposomes,<sup>12,38,39</sup> few have described the intracellular trafficking after intracellular uptake. Here, we showed that DXR forms a complex with P1TP and phospholipids, and that DXR was subject to intracellular trafficking as a complex in cells exposed to DXR-encapsulated liposomes. To our knowledge, there are no reports showing that liposomal lipids and encapsulated drugs form a complex with specific intracellular proteins, or that the intracellular trafficking of drugs requires complex formation. These findings demonstrate the importance of elucidating the interactions between encapsulated drugs and other intracellular proteins/liposomal components in order to improve the pharmacological activities and safety of encapsulated drugs.

It well-known that P1TP is involved in the intracellular trafficking of phospholipids from the ER/Golgi apparatus to the cell membrane.<sup>29,36,37</sup> Therefore, transport of DXR by P1TP–phospholipid complexes was responsible for the enhanced extracellular efflux of DXR. Moreover, because the cytotoxicity of DXR was increased by the suppression of P1TP expression (Figure 4C), it seems likely that DXR transport by P1TP–phospholipid complexes contributes to a decrease in the pharmacological effects of DXR. Because chols and PEG-modified phospholipids are not subject to intracellular transport by P1TP,<sup>18</sup> P1TP is unlikely to form a complex with either component, preventing an increase in the extracellular efflux of DXR via P1TP complexes. P1TP is involved in the transfer of lipid components between different membrane compartments and known as the conserved proteins in many cellular processes in various types of cells.<sup>37</sup> In the present study, we showed that

DXR formed a complex with P1TP and phospholipids and that DXR underwent intracellular trafficking as a complex in cells exposed to encapsulated DXR. These findings suggest that P1TP controls the efflux of encapsulated DXR and might provide a defensive mechanism against liposomal formulations in cancer cells. Taking these factors into consideration, to achieve potent pharmaceutical activities at low doses, the construction of liposomes lacking components that are subject to intracellular transport by P1TP is effective for suppressing the extracellular efflux of DXR. In future studies we intend to evaluate the effects of other liposomal components, including cationic phospholipids, to provide further insight into the design of liposomes capable of enhancing the pharmacological properties of the encapsulated agents.

In conclusions, we determined the intracellular trafficking mechanism of PEG-modified phospholipids *in vitro*, and showed that PEG modification affects the intracellular trafficking of the modified molecules. We next showed that DXR increased the expression of P1TP, ABCA1, and ABCB1, which are involved in the intracellular trafficking of phospholipids. DXR encapsulated into liposomes increased the extracellular efflux of liposomal phospholipids. We also found that the intracellular trafficking of DXR is controlled by P1TP, which forms a complex with phospholipids and DXR in DXR-encapsulated liposomes. DXR-encapsulated PEG-modified liposomes have already been approved for clinical use in several countries and are expected to be promising anticancer agents. To date, there have been very few reports describing the intracellular trafficking of PEG-modified phospholipids or DXR. We believe that our findings might help with efforts to prepare novel formulations of DXR, including encapsulation in PEG-modified liposomes, to enhance the therapeutic effects and reduce unexpected toxicity of DXR.

## ■ ASSOCIATED CONTENT

### 📄 Supporting Information

This material is available free of charge via the Internet at <http://pubs.acs.org>.

## ■ AUTHOR INFORMATION

### Corresponding Author

\*Telephone: +81-3-3700-9662. Fax: +81-3-3700-9662. E-mail: [kumikato@nihs.go.jp](mailto:kumikato@nihs.go.jp).

### Notes

The authors declare no competing financial interest.

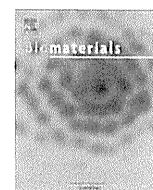
## ■ ACKNOWLEDGMENTS

This work was supported in part by Health and Labour Sciences Research Grants from the Ministry of Health, Labour and Welfare of Japan, and by KAKENHI Grant Number 24590070 from the Japan Society for the Promotion of Science.

## ■ REFERENCES

- (1) Adler-Moore, J.; Proffitt, R. T. AmBisome: liposomal formulation, structure, mechanism of action and pre-clinical experience. *J. Antimicrob. Chemother.* **2002**, *49*, 21–30.
- (2) Wang, X.; Andersson, R.; Ding, J.; Norgren, L.; Bengmark, S. Reticuloendothelial system function following acute liver failure induced by 90% hepatectomy in the rat. *HPB Surg.* **1993**, *6*, 151–162.
- (3) Allen, C.; Dos Santos, N.; Gallagher, R.; Chiu, G. N.; Shu, Y.; Li, W. M.; Johnstone, S. A.; Janoff, A. S.; Mayer, L. D.; Webb, M. S.; Bally, M. B. Controlling the physical behavior and biological performance of liposome formulations through use of surface grafted poly(ethylene glycol). *Biosci. Rep.* **2002**, *22*, 225–250.
- (4) Immordino, M. L.; Dosio, F.; Cattel, L. Stealth liposomes: review of the basic science, rationale, and clinical applications, existing and potential. *Int. J. Nanomed.* **2006**, *1*, 297–315.
- (5) Price, M. E.; Cornelius, R. M.; Brash, J. L. Protein adsorption to polyethylene glycol modified liposomes from fibrinogen solution and from plasma. *Biochim. Biophys. Acta* **2001**, *1512*, 191–205.
- (6) Allen, T. M. Long-circulating (sterically stabilized) liposomes for targeted drug delivery. *Trends Pharmacol. Sci.* **1994**, *15*, 215–220.
- (7) van Bochove, G. S.; Paulis, L. E.; Segers, D.; Mulder, W. J.; Krams, R.; Nicolay, K.; Strijkers, G. J. Contrast enhancement by differently sized paramagnetic MRI contrast agents in mice with two phenotypes of atherosclerotic plaque. *Contrast Media Mol. Imaging* **2011**, *6*, 35–45.
- (8) Gabizon, A.; Shmeeda, H.; Barenholz, Y. Pharmacokinetics of pegylated liposomal Doxorubicin: review of animal and human studies. *Clin. Pharmacokinet.* **2003**, *42*, 419–436.
- (9) Abraham, S. A.; Waterhouse, D. N.; Mayer, L. D.; Cullis, P. R.; Madden, T. D.; Bally, M. B. The liposomal formulation of doxorubicin. *Methods Enzymol.* **2005**, *391*, 71–97.
- (10) Tirosh, O.; Barenholz, Y.; Katzhendler, J.; Prieve, A. Hydration of polyethylene glycol-grafted liposomes. *Biophys. J.* **1998**, *74*, 1371–1379.
- (11) Terada, T.; Iwai, M.; Kawakami, S.; Yamashita, F.; Hashida, M. Novel PEG-matrix metalloproteinase-2 cleavable peptide-lipid containing galactosylated liposomes for hepatocellular carcinoma-selective targeting. *J. Controlled Release* **2006**, *111*, 333–342.
- (12) Hatakeyama, H.; Akita, H.; Ishida, E.; Hashimoto, K.; Kobayashi, H.; Aoki, T.; Yasuda, J.; Obata, K.; Kikuchi, H.; Ishida, T.; Kiwada, H.; Harashima, H. Tumor targeting of doxorubicin by anti-MT1-MMP antibody-modified PEG liposomes. *Int. J. Pharm.* **2007**, *342*, 194–200.
- (13) Sakai-Kato, K.; Ishikura, K.; Oshima, Y.; Tada, M.; Suzuki, T.; Ishii-Watabe, A.; Yamaguchi, T.; Nishiyama, N.; Kataoka, K.; Kawanishi, T.; Okuda, H. Evaluation of intracellular trafficking and clearance from HeLa cells of doxorubicin-bound block copolymers. *Int. J. Pharm.* **2012**, *423*, 401–409.
- (14) Fardel, O.; Lecœur, V.; Daval, S.; Corlu, A.; Guillouzo, A. Up-regulation of P-glycoprotein expression in rat liver cells by acute doxorubicin treatment. *Eur. J. Biochem.* **1997**, *246*, 186–192.
- (15) Mercier, C.; Declèves, X.; Masseguin, C.; Fragner, P.; Tardy, M.; Roux, F.; Gabrion, J.; Scherrmann, J. M. P-glycoprotein (ABCB1) but not multidrug resistance-associated protein 1 (ABCC1) is induced by doxorubicin in primary cultures of rat astrocytes. *J. Neurochem.* **2003**, *87*, 820–830.
- (16) Shukla, A.; Hillegass, J. M.; MacPherson, M. B.; Beuschel, S. L.; Vacek, P. M.; Pass, H. I.; Carbone, M.; Testa, J. R.; Mossman, B. T. Blocking of ERK1 and ERK2 sensitizes human mesothelioma cells to doxorubicin. *Mol. Cancer* **2010**, *9*, 314.
- (17) Bao, L.; Haque, A.; Jackson, K.; Hazari, S.; Moroz, K.; Jetly, R.; Dash, S. Increased expression of P-glycoprotein is associated with doxorubicin chemoresistance in the metastatic 4T1 breast cancer model. *Am. J. Pathol.* **2011**, *178*, 838–852.
- (18) Un, K.; Sakai-Kato, K.; Oshima, Y.; Kawanishi, T.; Okuda, H. Intracellular trafficking mechanism, from intracellular uptake to extracellular efflux, for phospholipid/cholesterol liposomes. *Biomaterials* **2012**, *33*, 8131–8141.
- (19) Bangham, A. D.; Standish, M. M.; Watkins, J. C. Diffusion of univalent ions across the lamellae of swollen phospholipids. *J. Mol. Biol.* **1965**, *13*, 238–252.
- (20) Fritze, A.; Hens, F.; Kimpfler, A.; Schubert, R.; Peschka-Süss, R. Remote loading of doxorubicin into liposomes driven by a transmembrane phosphate gradient. *Biochim. Biophys. Acta* **2006**, *1758*, 1633–1640.
- (21) Rejman, J.; Bragonzi, A.; Conese, M. Role of clathrin- and caveolae-mediated endocytosis in gene transfer mediated by lipo- and polyplexes. *Mol. Ther.* **2005**, *12*, 468–474.

- (22) Perez, A. P.; Cosaka, M. L.; Romero, E. L.; Morilla, M. J. Uptake and intracellular traffic of siRNA dendriplexes in glioblastoma cells and macrophages. *Int. J. Nanomed.* **2011**, *6*, 2715–2728.
- (23) Johansson, M.; Bocher, V.; Lehto, M.; Chinetti, G.; Kuismanen, E.; Ehnholm, C.; Staels, B.; Olkkonen, V. M. The two variants of oxysterol binding protein-related protein-1 display different tissue expression patterns, have different intracellular localization, and are functionally distinct. *Mol. Biol. Cell* **2003**, *14*, 903–915.
- (24) Hölttä-Vuori, M.; Alpy, F.; Tanhuanpää, K.; Jokitalo, E.; Mutka, A. L.; Ikonen, E. MLN64 is involved in actin-mediated dynamics of late endocytic organelles. *Mol. Biol. Cell* **2005**, *16*, 3873–86.
- (25) Koivusalo, M.; Jansen, M.; Somerharju, P.; Ikonen, E. Endocytic trafficking of sphingomyelin depends on its acyl chain length. *Mol. Biol. Cell* **2007**, *18*, 5113–5123.
- (26) Xu, S.; Benoff, B.; Liou, H. L.; Lobel, P.; Stock, A. M. Structural basis of sterol binding by NPC2, a lysosomal protein deficient in Niemann-Pick type C2 disease. *J. Biol. Chem.* **2007**, *282*, 23525–23531.
- (27) Hanada, K.; Kumagai, K.; Tomishige, N.; Kawano, M. CERT and intracellular trafficking of ceramide. *Biochim. Biophys. Acta* **2007**, *1771*, 644–653.
- (28) Jensen, D.; Schekman, R. COPII-mediated vesicle formation at a glance. *J. Cell Sci.* **2011**, *124*, 1–4.
- (29) Hsuan, J.; Cockcroft, S. The PITP family of phosphatidylinositol transfer proteins. *Genome Biol.* **2001**, *2*, 1–8.
- (30) Hynynen, R.; Suchanek, M.; Spandl, J.; Bäck, N.; Thjele, C.; Olkkonen, V. M. OSBP-related protein 2 is a sterol receptor on lipid droplets that regulates the metabolism of neutral lipids. *J. Lipid Res.* **2009**, *50*, 1305–1315.
- (31) Kimura, Y.; Morita, S. Y.; Matsuo, M.; Ueda, K. Mechanism of multidrug recognition by MDR1/ABCB1. *Cancer Sci.* **2007**, *98*, 1303–1310.
- (32) Rose, P. G. Pegylated liposomal doxorubicin: optimizing the dosing schedule in ovarian cancer. *Oncologist* **2005**, *10*, 205–214.
- (33) Smit, J. W.; Duin, E.; Steen, H.; Oosting, R.; Roggeveld, J.; Meijer, D. K. Interactions between P-glycoprotein substrates and other cationic drugs at the hepatic excretory level. *Br. J. Pharmacol.* **1998**, *123*, 361–370.
- (34) Kondratov, R. V.; Komarov, P. G.; Becker, Y.; Ewenson, A.; Gudkov, A. V. Small molecules that dramatically alter multidrug resistance phenotype by modulating the substrate specificity of P-glycoprotein. *Proc. Natl. Acad. Sci. U.S.A.* **2001**, *98*, 14078–14083.
- (35) Shen, F.; Chu, S.; Bence, A. K.; Bailey, B.; Xue, X.; Erickson, P. A.; Montrose, M. H.; Beck, W. T.; Erickson, L. C. Quantitation of doxorubicin uptake, efflux, and modulation of multidrug resistance (MDR) in MDR human cancer cells. *J. Pharmacol. Exp. Ther.* **2008**, *324*, 95–102.
- (36) Ségui, B.; Allen-Baume, V.; Cockcroft, S. Phosphatidylinositol transfer protein beta displays minimal sphingomyelin transfer activity and is not required for biosynthesis and trafficking of sphingomyelin. *Biochem. J.* **2002**, *366*, 23–34.
- (37) Garner, K.; Hunt, A. N.; Koster, G.; Somerharju, P.; Groves, E.; Li, M.; Raghu, P.; Holic, R.; Cockcroft, S. Phosphatidylinositol transfer protein, cytoplasmic 1 (PITPNC1) binds and transfers phosphatidic acid. *J. Biol. Chem.* **2012**, *287*, 32263–32276.
- (38) Li, X.; Ding, L.; Xu, Y.; Wang, Y.; Ping, Q. Targeted delivery of doxorubicin using stealth liposomes modified with transferrin. *Int. J. Pharm.* **2009**, *373*, 116–123.
- (39) Jung, S. H.; Jung, S. H.; Seong, H.; Cho, S. H.; Jeong, K. S.; Shin, B. C. Polyethylene glycol-complexed cationic liposome for enhanced cellular uptake and anticancer activity. *Int. J. Pharm.* **2009**, *382*, 254–261.



## Leading opinion

# Elucidating the molecular mechanism for the intracellular trafficking and fate of block copolymer micelles and their components



Kumiko Sakai-Kato<sup>a,\*</sup>, Keita Un<sup>a</sup>, Kunie Nanjo<sup>a</sup>, Nobuhiro Nishiyama<sup>b</sup>,  
Hiroyuki Kusuhara<sup>c</sup>, Kazunori Kataoka<sup>d,e</sup>, Toru Kawanishi<sup>f</sup>, Yukihiro Goda<sup>a</sup>,  
Haruhiro Okuda<sup>f</sup>

<sup>a</sup> Division of Drugs, National Institute of Health Sciences, 1-18-1 Kamiyoga, Setagaya-ku, Tokyo 158-8501, Japan

<sup>b</sup> Polymer Chemistry Division, Chemical Resources Laboratory, Tokyo Institute of Technology, R1-11, 4259 Nagatsuda, Midori, Yokohama 226-8503, Japan

<sup>c</sup> Laboratory of Molecular Pharmacokinetics, Graduate School of Pharmaceutical Sciences, The University of Tokyo, 7-3-1 Hongo, Bunkyo, Tokyo 113-0033, Japan

<sup>d</sup> Center for Disease Biology and Integrative Medicine, Graduate School of Medicine, The University of Tokyo, 7-3-1 Hongo, Bunkyo, Tokyo 113-0033, Japan

<sup>e</sup> Department of Materials Engineering, Graduate School of Engineering, The University of Tokyo, 7-3-1 Hongo, Bunkyo, Tokyo 113-8656, Japan

<sup>f</sup> National Institute of Health Sciences, 1-18-1 Kamiyoga, Setagaya-ku, Tokyo 158-8501, Japan

## ARTICLE INFO

## Article history:

Received 17 October 2013

Accepted 8 November 2013

Available online 2 December 2013

## Keywords:

Block copolymer micelles

Intracellular trafficking

Intermembrane transport

NPC1

ORP2

ABCB1

## ABSTRACT

Block copolymer micelles have shown promise for the intracellular delivery of chemotherapeutic agents, proteins, and nucleic acids. Understanding the mechanism of their intracellular trafficking and fate, including the extracellular efflux of the polymers, will help improve their efficacy and minimize their safety risks. In this Leading Opinion paper, we discuss the molecular mechanism of block copolymer micelle trafficking, from intracellular uptake to extracellular efflux, on the basis of studies with HeLa cells. By using FRET (fluorescence resonance energy transfer) with confocal microscopy, we found that, following their intracellular transport via endocytosis, the micelles dissociated into their polymeric components in late endosomes and/or lysosomes. Furthermore, we confirmed that the intrinsic proteins NPC1 and ORP2 are involved in the intermembrane transfer of polymers from the endosome to the plasma membrane via the ER (endoplasmic reticulum) by using knockdown experiments with siRNAs. After the polymers were transported to the plasma membrane with the aid of ORP2, they were extruded into the cell medium via ABC transporter, ABCB1. Experiments with ABCB1-expressing vesicles indicated that the polymer itself, and not the fluorescent compounds, was recognized by the transporter. These findings, and the analysis of related mechanisms, provide valuable information that should help minimize the potential risks associated with the intracellular accumulation of block copolymer micelles and to improve their therapeutic efficacy.

© 2013 Elsevier Ltd. All rights reserved.

## 1. Introduction

Drug delivery systems that use nanometer-sized carriers show promise for the targeted transfer of chemotherapeutic agents, proteins, and nucleic acids to tissues or organs. Nanomaterials have been extensively studied as drug carriers, and some formulations for cancer treatment have been applied clinically [1–3]. Block copolymer micelles have recently received considerable attention as targetable carrier systems [4–7]. The formulation of block copolymer micelles can alter the pharmacokinetic characteristics such as the volume of distribution, clearance, half-life, and tissue

distribution of the active substances included [8–10]. Moreover, finely tuning the design of the block copolymers can increase their longevity in the bloodstream and allow the controlled release of the drugs, which consequently improves the pharmacodynamics of the drugs and/or avoids systemic toxicity.

The development of these drug carriers for the cellular uptake of therapeutic proteins and nucleic acids is of particular interest. Because nucleic acids, proteins, and peptides are not taken up into cells via passive diffusion, their intracellular uptake by nanocarriers is a key to targeting the delivery of these compounds at the cellular or organelle level. Specifically, the incorporation of these compounds into nanocarriers will improve the efficiency of their intracellular uptake or delivery to specific organelle, thereby ensuring their therapeutic effects. Furthermore, clarifying the intracellular trafficking mechanisms may also facilitate the

\* Corresponding author. Tel./fax: +81 3 3700 9662.

E-mail address: [kumikato@mhs.go.jp](mailto:kumikato@mhs.go.jp) (K. Sakai-Kato).

discovery of new drug delivery strategies, such as targeting to specific cell organelles. Thus, to improve the efficiency of the intracellular uptake of these compounds, it is essential to understand the detailed mechanism of their trafficking including the fate of the micelles and their component polymers after their uptake via endocytosis. To this end, the use of covalently bound fluorescent reagents as probes has gradually shed light on the internalization pathways and intracellular localizations of polymeric nanoparticulate carriers [11–13].

In parallel, the safety of these carriers must be investigated. To ensure that these materials are safe, it is essential to know whether the components of the carriers are accumulated inside the cell or undergo sequestration (i.e., metabolism or efflux). The potential long-term effects of these novel polymers when used as nanosized particles have not yet been determined. To address this issue, we investigated the intracellular fate of polymer micelles conjugated with doxorubicin (Dox) in HeLa cells [14]. We demonstrated that Dox is endocytosed and localized to the endoplasmic reticulum, and that an ABC transporter, ABCB1, is involved in the efflux of the polymer from these cells. However, many factors remain unknown, for example, where do the micelles dissociate into their constituent polymers after internalization? What are the molecular mechanisms involved in trafficking to each organelle and in the efflux of polymers or micelles? Moreover, the trafficking phenomenon we found previously was limited to the case of Dox-conjugated polymers. Questions remain regarding the trafficking of other block copolymers, for example, those conjugated with different compounds or those with different poly(ethylene glycol) (PEG) lengths.

In the present study, we constructed three micelles by using three block copolymers (doxorubicin, Nile Red, and DBD (4-(*N,N*-dimethylsulfamoyl)-2,1,3-benzoxadiazole)) with different poly(ethylene glycol) (PEG) lengths (Mw 5000 or 12,000), detailed descriptions of which can be found in Section 3.1. To investigate the structural integrity of the micelles inside the cells, fluorescence resonance energy transfer (FRET) micelles were also constructed by using two types of polymers, that is, polymers with covalently bound Nile Red and polymers with covalently bound DBD. The trafficking of the micelles and their components, from intracellular uptake to extracellular efflux, was evaluated and the intrinsic molecules involved in the trafficking process were identified.

## 2. Materials and methods

### 2.1. Materials

Poly(ethylene glycol)-poly(aspartate) (PEG-P(Asp)) block copolymers with conjugated Dox were synthesized by Nippon Kayaku Co., Ltd. (Tokyo, Japan) [15]. Dextran (Dextran Texas Red, Molecular weight 10,000), polystyrene particles (FluoSphere Red, average particle size; 40.1 nm), Dulbecco's modified Eagle's Medium (DMEM), RPMI-1640, penicillin/streptomycin, and Opti-MEM I were purchased from Life Technologies (Brooklyn, NY, USA). Fetal bovine serum (FBS) was obtained from Nichirei Biosciences (Tokyo, Japan). Fluorescently labeled amorphous silica particles (Sicstar RedF, average particle size; 45.5 nm) were obtained from Micromod Partikeltechnologie (Rostock, Germany). Isolated mammalian cell membranes containing human ABCB1, for vesicle transport assays, (SB-MDR1-K-VT) were purchased from SOLVO Biotechnology (Hungary). All chemicals used in this study were of the highest purity available. HeLa cells (Health Science Research Resources Bank, Osaka, Japan) were cultured in DMEM. The medium was supplemented with 10% FBS, 100 U/mL penicillin/streptomycin. Cells were grown in a humidified incubator at 37 °C/5% CO<sub>2</sub>.

### 2.2. Synthesis of the DBD-conjugated polymer and Nile Red-conjugated polymer

Poly(ethylene glycol)-poly(aspartate) block copolymer (PEG-P(Asp)) was obtained as described previously [15]. The degree of polymerization of PEG-P(Asp) was determined to be 35–45 by neutralization titration (Supplementary Fig. 1–1).

For the synthesis of DBD-conjugated polymer, PEG-P(Asp) (100 mg) and dimethylaminopyridine (23 mg, 0.8 equiv. for COOH) were dissolved in DMF (1.5 mL) and then DBD-ED (13 mg, 0.2 equiv.) and 4-phenyl-1-butanol (25  $\mu$ L, 0.7 equiv.) were added. Diisopropylcarbodiimide (36  $\mu$ L, 1.0 equiv.) was added to the solution and stirred at room temperature for 5 h. Diisopropylcarbodiimide (36  $\mu$ L, 1.0 equiv.) was added again and the solution was stirred for 18 h. The reaction mixture was then

dropped into a mixture of ethyl acetate and hexane (1:3). The resulting precipitate was filtered, washed with the mixture of ethyl acetate and hexane (1:3), and dried under vacuum to obtain the DBD-conjugated polymer (99 mg) as a powder. <sup>1</sup>H NMR spectra in DMSO-d<sub>6</sub> and the assignment are shown in Supplementary Fig. 1–2.

For the synthesis of the Nile Red-conjugated polymer, PEG-P(Asp) (100 mg) and dimethylaminopyridine (28 mg, 1.0 equiv.) were dissolved in DMF (1.5 mL) and then Nile-Red (8.8 mg, 0.1 equiv.) and 4-phenyl-1-butanol (36  $\mu$ L, 1.0 equiv.) were added. Diisopropylcarbodiimide (36  $\mu$ L, 1.0 equiv.) was added to the solution, which was then stirred at room temperature for 18 h. The reaction mixture was dropped into a mixture of ethyl acetate and hexane (1:3). The resulting precipitate was filtered, washed with the mixture of ethyl acetate and hexane (1:3), and dried under vacuum to obtain the Nile Red-conjugated polymer (109 mg) as a powder. <sup>1</sup>H NMR spectra in DMSO-d<sub>6</sub> and the assignment are shown in Supplementary Fig. 1–3.

### 2.3. Physicochemical properties of block copolymer micelles

The particle size and polydispersity index (PDI) of the block copolymer micelles were determined with a Zetasizer Nano ZS instrument (Malvern Instruments, Worcestershire, UK).

### 2.4. Evaluation of the intracellular trafficking of block copolymer micelles

To quantify the intracellular uptake of the polymers, we used a final polymer concentration of 50  $\mu$ g/mL in this study. HeLa cells ( $5 \times 10^4$ ) were seeded onto 6-well plates in medium containing 10% FBS and 100 U/mL penicillin/streptomycin. After incubation for 24 h at 37 °C/5% CO<sub>2</sub>, the cells were exposed to 50  $\mu$ g/mL micelles in culture medium. After incubation for pre-determined durations, the incubation medium was replaced with Hanks' balanced salt solution (HBSS). The cells were trypsinized with 0.25% trypsin-ethylenediamine tetraacetic acid (EDTA) (Life Technologies), washed with HBSS three times, and suspended in lysis buffer (1.0% Triton X-100 in HBSS). The cell suspension was then shaken and centrifuged (15,000 $\times$  g, 4 °C, 10 min). The fluorescence intensity of the resultant supernatant was measured on a fluorescence spectrophotometer (F-7000; Hitachi High-Technologies, Tokyo, Japan) using 440 nm excitation and 580 nm emission for DBD-conjugated polymers, 580 nm excitation and 640 nm emission for Nile Red-conjugated polymers, and 470 nm excitation and 590 nm emission for Dox-conjugated polymers. The fluorescence intensity was normalized with respect to the protein content of the cells. The protein concentration was determined by using a Protein Assay Kit (Bio-Rad Laboratories, Hercules, CA, USA).

### 2.5. Confocal microscopy

To observe the colocalization of block copolymer micelles with the intracellular compartment, specific intracellular compartment components were labeled by using fluorescent dyes. All dyes for confocal microscopy were purchased from Life Technologies and used in accordance with the manufacturer's instructions. Endosomes were labeled with transferrin conjugated to Alexa Fluor 488 or Alexa Fluor 594, and lysosomes were labeled with LysoTracker Green DND-26 or LysoTracker Red DND-99. The ER was labeled with ER-Tracker Green or ER-Tracker Red, and the Golgi apparatus was labeled with Bodipy-FL C5-ceramide or Bodipy-TR C5-ceramide complexed to BSA. Confocal microscopy was performed as previously described [14]. Briefly, cells ( $1.0 \times 10^5$ ) were plated on 35-mm glass-bottom dishes coated with poly-L-lysine (Matsunami Glass, Osaka, Japan) in medium containing 10% FBS and 100 U/mL penicillin/streptomycin. After incubation for 24 h, cells were exposed to 50  $\mu$ g/mL micelles in culture medium. At a pre-determined time after addition of the micelles, cells were washed and kept in HBSS for imaging with a confocal microscope (Carl Zeiss LSM 510; Carl Zeiss Microscopy GmbH, Germany). Pseudocolor luminescent images were captured using LSM Image Browser (Carl Zeiss Microscopy GmbH, Germany).

An FRET experiment was performed using FRET micelles composed of DBD-conjugated polymers and Nile Red polymers (9:1, w:w). Cells were exposed to 50  $\mu$ g/mL FRET micelles in culture medium. Two hours after addition of the micelles, cells were washed and kept in medium without micelles and then imaged with a confocal microscope at 2, 10, and 24 h after addition of the micelles.

### 2.6. Endocytosis inhibition and Golgi destruction

To investigate the mechanism of endocytosis of the prepared micelles, 10  $\mu$ g/mL chlorpromazine (a clathrin-mediated endocytosis inhibitor), 150  $\mu$ M genistein or 2.0 mM methyl- $\beta$ -cyclodextrin (M $\beta$ CD) (caveolae-mediated endocytosis inhibitors), or 50  $\mu$ M 5-(*N*-ethyl-*N*-isopropyl) amiloride (a macropinocytosis inhibitor) were used [16,17]. Each endocytosis inhibitor was added to the culture medium 30 min before the addition of the micelles. To inhibit ER-to-Golgi transfer, to investigate whether ER-to-Golgi transfer is involved in the intracellular trafficking of micelles or polymers, cells were incubated in medium containing 1  $\mu$ g/mL brefeldin A 30 min before the addition of the micelles [18].

### 2.7. Small interfering RNA (siRNA) transfer

To clarify which intrinsic proteins are involved in the intracellular trafficking and efflux of the polymers, the expression of specific proteins was down-regulated by

using siRNA. Stealth RNAi oligonucleotides (25-mer, Life Technologies), which unlike conventional siRNAs can reduce the cytotoxic interferon response [19], were obtained from Life Technologies. The siRNA sequences used in this study are shown in Table 1. As a negative control, the Stealth RNAi High GC Negative Control Duplex (Life Technologies) was used [14]. The Stealth RNAi oligonucleotides were transfected into cells by using Lipofectamine RNAiMAX (Life Technologies) according to the manufacturer's protocols. Briefly, the cells were incubated for 24 h. Each siRNA was then added, and the cells were incubated for a further 48 h, at which time the micelles (50 µg/mL) were added. Western blotting was used to confirm the down-regulation of each protein as described previously [14]. After the cells were incubated with the micelles, the culture medium was replaced with HBSS. Cells were trypsinized and lysed to quantify the intracellular amount of polymer as described above (Section 2.3).

### 2.8. Transport experiment

To investigate ATP-dependent transport, mammalian cell membrane vesicles expressing ABCB1 were used according to the manufacturer's instructions. Suspensions of vesicles expressing ABCB1, and control vesicles without ABCB1 (50 µL each), were plated on a 96-well plate. Samples (0.75 µL) at the indicated concentration and reaction buffer (25 µL) were added to each well, and the plates were incubated at 37 °C for 5 min. After washing by centrifugation (1500× g, 5 min, 4 °C), the fluorescence intensity of the polymers after intravesicular transport was measured using a fluorescence spectrophotometer as described in Section 2.3. The fluorescence intensity of intravesicular polymers incubated with MgATP was subtracted from that of polymers incubated without MgATP.

### 2.9. Statistical analyses

Results are presented as the mean ± SD of more than three experiments. Analysis of variance was used to test the statistical significance of the differences among groups. Two-group comparisons were performed with a Student's *t*-test. Multiple comparisons between control and test groups were performed with a Dunnett's test.

## 3. Results

### 3.1. Chemical structures of block copolymers and physicochemical properties

We used three different kinds of micelles formed from Dox-conjugated, DBD-conjugated, and Nile Red-conjugated PEG–P(Asp) block copolymers, respectively (Supplementary Fig. 1), hereinafter referred to as Dox-conjugated polymers, DBD-conjugated polymers, and Nile Red-conjugated polymers, respectively. Dox-conjugated polymers consisted of PEG ( $M_w \sim 5000$ ) and P(Asp) (polymerization degree, 30) with partially conjugated doxorubicin (ca. 45%) to the side chain of the P(Asp) [15]. DBD-conjugated polymers consist of PEG ( $M_w \sim 12,000$ ) and P(Asp) (polymerization degree, 35–45), with partially conjugated DBD (ca. 10%) and 4-phenyl-1-butanol (ca. 43%) to increase the hydrophobicity to the side chain of the P(Asp). Nile Red-conjugated polymers consist of PEG ( $M_w \sim 12,000$ ) and P(Asp) (polymerization degree, 35–45) with partially conjugated Nile Red (ca. 10%) and 4-phenyl-1-butanol (ca. 53%) to increase the hydrophobicity to the side chain of the P(Asp). When these block copolymers were dissolved in aqueous medium, they spontaneously formed micelles with

**Table 2**

Particle sizes and PDI of block copolymer micelles used in this study.

	Particle size	PDI
DBD-conjugated polymer micelles	31.7 ± 0.11	0.180 ± 0.011
NR-conjugated polymer micelles	31.4 ± 0.67	0.184 ± 0.006
Dox-conjugated polymer micelles	32.3 ± 0.19	0.180 ± 0.014
DBD:NR (9:1)-conjugated polymer micelles	32.4 ± 0.18	0.198 ± 0.005

Each value represents the mean ± S.D. ( $n = 3$ ).

hydrophobic cores. We constructed FRET micelles by mixing DBD-conjugated polymers with Nile Red-conjugated polymers. The particle sizes of the resultant micelles (~30 nm) are shown in Table 2.

### 3.2. Endocytosis of block copolymers

To investigate the intracellular transport mechanisms of the micelles and their components, we used confocal microscopy to observe the intracellular trafficking of fluorescent micelles composed of Dox-, Nile Red- or DBD-conjugated polymers. All three of the different types of fluorescent micelle colocalized with the endosomes after 1 h in HeLa cells (Fig. 1A). At 2 h-post-incubation, most of the micelles colocalized with the lysosomes although some were distributed outside the vesicles (Fig. 1B).

The use of endocytosis inhibitors to clarify the endocytosis mechanism demonstrated that the internalized amounts of fluorescent micelles in HeLa cells were significantly suppressed at 2, 24 and 48 h in the presence of chlorpromazine (Fig. 2). Genistein and MβCD also inhibited the intracellular uptake of all of the micelles at 24 and 48 h, although the extent of inhibition was less in the case of genistein and MβCD compared with that of chlorpromazine. These results indicate that the intracellular uptake of the micelles proceeded mainly through clathrin-mediated endocytosis. Caveolae-mediated endocytosis also contributed to the uptake over time.

### 3.3. Dissociation of micelles into polymers in HeLa cells

We then attempted to identify the intracellular location where the block copolymer micelles dissociate into polymers after internalization. We constructed an FRET system to track the structural integrity of the micelles once they were internalized into the HeLa cells. FRET is a distance-dependent process in which excitation energy is absorbed by a molecular fluorophore (the donor) and then transferred to a nearby fluorophore (the acceptor). It is a highly sensitive technique for investigating biological phenomena that produce changes in molecular proximity [20,21]. We used micelles consisting of DBD-conjugated polymers and Nile Red-conjugated polymers (9:1, w/w; Fig. 3A). The mixing ratio of 9:1 of DBD-:Nile Red-conjugated polymers resulted in the formation of

**Table 1**

The siRNA sequences used in this study.

Target gene	Sense strand	Antisense strand
MLN64	5'-GCUGA AGGAU UAAAC AAUGA CUUCA-3'	5'-UGAAG UCAUU GUUUA AUCCU UCAGC-3'
ORP1	5'-GCACC UCUGA GGAGU UGGAU GAAAU-3'	5'-AUUUC AUCCA ACUCC UCAGA GGUGC-3'
NPC1	5'-CCCUC GUCCU GGAUC GACGA UUAUU-3'	5'-AAUAA UCGUC GAUCC AGGAC GAGGG-3'
CERT	5'-ACGUG AGAAG UUGCG UGAAA UGGA-3'	5'-UUCCA UUUCA GCCAA CUUCU CACGU-3'
Sec31A	5'-CCAGG CCAAU AAGCU GGGUG UCUA-3'	5'-UUAGA CACCC AGCUU AUUGG CCUGG-3'
ORP2	5'-GAGAG GAGAG GUGAC CACCU GAGAA-3'	5'-UUCUC AGGUG GUCAC CUCUC CUCUC-3'
PITP	5'-GGAUA UUUAC AAACU UCCAU CGCCA-3'	5'-UGGCG AUGGA AGUUU GUAAA UAUC-3'
ABCA1	5'-UUUAG AUGCU GGACA CUGCC AAGGC-3'	5'-GCCUU GGCAG UGUCC AGCAU CUAAA-3'
ABCB1	5'-UCCCG UAGAA ACCUU ACAUU UAUGG-3'	5'-CCAUA AAUGU AAGGU UUCUA CGGA-3'
ABCC1	5'-CCGGU CUUUU CCAU UUCA CGAGA-3'	5'-UCUCG UUGAA AUGGG AAUAG ACCGG-3'
ABCG1	5'-UCUCG CUGAU GAAAG GGUC GCUCA-3'	5'-UGAGC GAGCC CUUUC AUCAG CGAGA-3'
Snap-25	5'-CAUGG AGAAG GCUCA UUCA ACAA-3'	5'-UUUGU UGAA UCAGC CUUCU CCAUG-3'

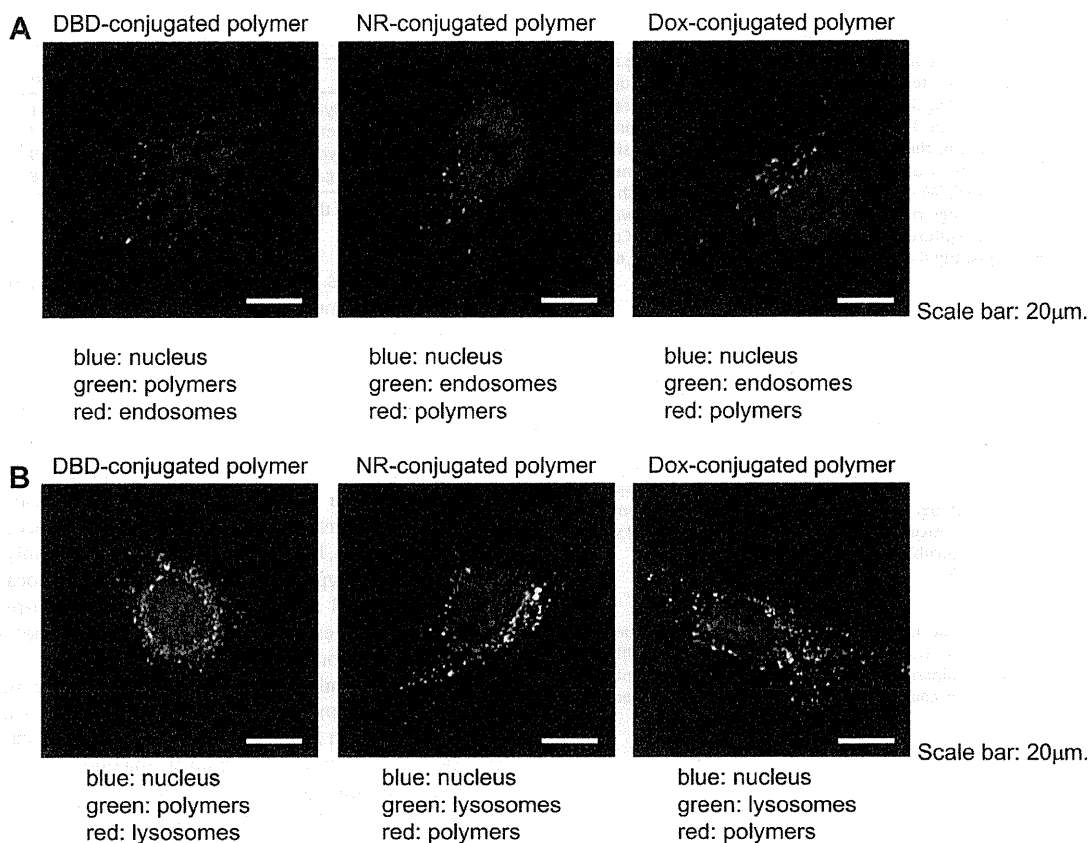


**Fig. 1.** (A) Confocal images showing the intracellular transport of micelles at 1 h after the addition of the micelles to HeLa cells. The endosomes are labeled with Alexa Fluor-conjugated transferrin. Scale bars = 20  $\mu$ m. (B) Confocal images showing the intracellular transport of micelles at 2 h after the addition of the micelles to HeLa cells. The lysosomes are labeled with LysoTracker Red or Green. Scale bars = 20  $\mu$ m.

block copolymer micelles with the most effective FRET efficiency. At 2 h after the addition of the micelles, we washed the cells with fresh medium to stop any further entry of micelles into the HeLa cells, whereupon only red (in web version) fluorescence was observed in the vesicular structure (Fig. 3B). Together with the result of the cellular uptake experiments, these results show that the block copolymers mostly maintain their micellar structure for at least 2 h after their internalization. Confocal microscopy images were taken at time intervals up to 24 h after the addition of the micelles. The fluorescence of the vesicular structures changed to yellow (in web version) after 10 h and then to green (in web version) after 24 h suggesting that the micelles gradually dissociated into polymers upon localization in the endosomes and/or lysosomes (Fig. 3B).

### 3.4. Intracellular trafficking of block copolymers

Using confocal microscopy, we further examined the intracellular trafficking of block copolymers with conjugated fluorescent compounds after their internalization. The fluorescence of all three polymers was colocalized to the ER, but not to the Golgi apparatus of the HeLa cells (Fig. 4). This is consistent with our previous study showing that Dox-bound micelles colocalize to the ER but not to the Golgi apparatus [14].

### 3.5. Molecular mechanisms of intracellular trafficking from endosomes/lysosomes to the cytoplasm and ER

In the case of cholesterol, there is some evidence for a direct pathway from endosomes to the ER [22,23]. We, therefore,

investigated whether the molecular mechanisms involved in the transport of cholesterol or other lipid analogs are also implicated in the intracellular trafficking of block copolymers. To elucidate the molecular mechanisms of block copolymer transport in HeLa cells, we used siRNAs to down-regulate the expression of specific lipid transport proteins. We hypothesized that the suppression of specific intracellular transport processes would decrease the extracellular efflux of the block copolymers, thereby leading to an increase in the intracellular amounts of each polymer. Fig. 5A shows the intracellular components and the typical lipid transport proteins we investigated. At 48 h after transfection with stealth RNAs, the expression of each protein was down-regulated in HeLa cells, which allowed us to investigate the role of these proteins in polymer transport (Supplementary Fig. 2). Initially, we investigated lipid transport proteins that are involved in intracellular trafficking from endosomes/lysosomes to other compartments, including the ER. These proteins included metastatic lymph-node gene 64 protein (MLN64) [24], oxysterol-binding protein-related protein 1 (ORP1) [25], and Niemann–Pick C1 protein (NPC1) [26,27]. Fig. 5B shows the amounts of intracellular polymer increased upon suppression of NPC1 expression. Confocal microscopy also revealed that the transport of polymers from endosomes or lysosomes to the ER was suppressed when NPC1 expression was knocked-down (Fig. 5C). These results suggest that NPC1 partially controls the intracellular trafficking of the polymers from the endosomes or lysosomes to the ER. On the other hand, they also indicate that MLN64 and ORP1, which are sterol-binding proteins that are involved in organizing late endosomal membrane trafficking, are not involved in the trafficking of these polymers. To determine



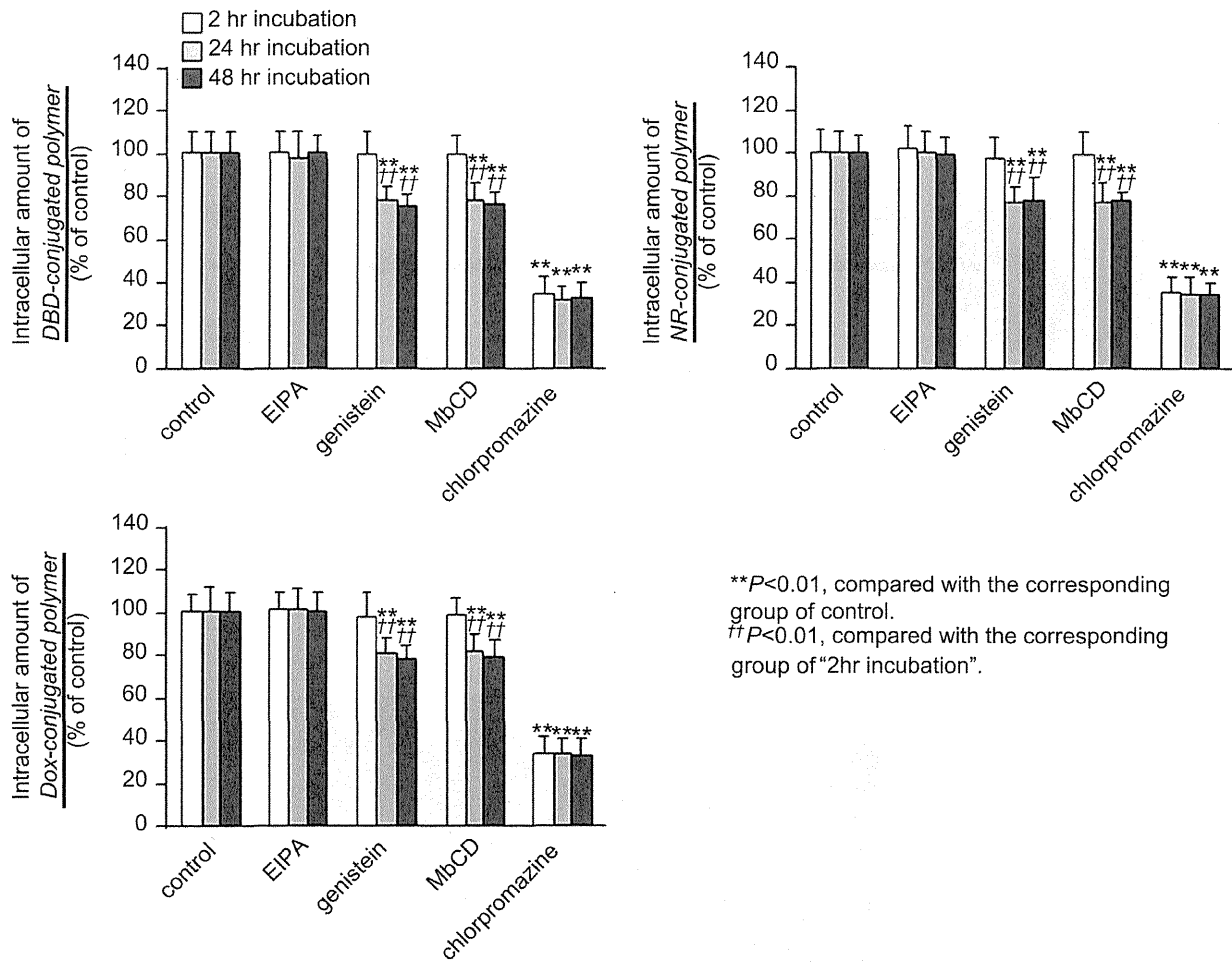


**Fig. 2.** The effect of endocytosis inhibitors on the intracellular amounts of polymers. The intracellular transport of micelles was evaluated at 2, 24, and 48 h after the addition of micelles to HeLa cells. Each endocytosis inhibitor was added to the cells 30 min before the addition of the micelles. \*\* $P < 0.01$  compared with the corresponding control group. †† $P < 0.01$ , compared with the corresponding group of "cells incubated for 2 h". Each value represents the mean  $\pm$  SD ( $n = 6$ ).

whether the absence of NPC1 also leads to increased retention of other polymers or nanoparticles that are internalized via endocytosis, we tested dextran, polystyrene nanoparticle, and silica nanoparticle. We found that the amounts of intracellular dextran, polystyrene nanoparticles, and silica nanoparticles were not affected by the suppression of NPC1 expression (Supplementary Fig. 3). These results thus show that NPC1 is not involved in trafficking of all polymers or nanoparticles from NPC1-positive late endosomes.

ER-to-Golgi transport is a major trafficking route for lipid molecules. Therefore, we investigated the involvement of ER-to-Golgi transport in the intracellular trafficking of block copolymers by examining whether trafficking was affected if ER-to-Golgi transport-related proteins were inhibited. We selected CERT, a known ceramide-transfer protein [28,29], and sec31A, a component of COPII that is required for the budding of vesicles from the ER [30,31] (Fig. 5A) for this assessment. The intracellular amounts of polymer were not affected by CERT or sec31A knockdown (Supplementary Fig. 4A), nor were they affected by the presence of brefeldin A, an inhibitor of the transport pathway from the ER to the Golgi apparatus [18] (Supplementary Fig. 4B). These results suggest that the ER-to-Golgi transport system is not involved in polymer trafficking, which is consistent with our results indicating that the polymers did not localize to the Golgi apparatus (Fig. 4B).

### 3.6. Molecular mechanism for the extracellular efflux of polymers

To investigate the transport of polymers to the plasma membrane, we examined oxysterol-binding protein-related protein 2 (ORP2) [32–34] and phosphatidylinositol transfer protein (PITP) [35–37]. These proteins are both involved in the intracellular transport of lipid molecules (Fig. 5A). Knockdown experiments using siRNAs against each protein revealed that the intracellular amounts of all three polymers did not change with the suppression of PITP, but increased upon the suppression of ORP2, a molecule involved in the trafficking of endogenous cholesterol (Fig. 6). On the other hand, the intracellular amounts of dextran, silica nanoparticles, and polystyrene nanoparticles were not affected by the suppression of ORP2 expression. (Supplementary Fig. 5A).

We previously reported that ABCB1, a member of the ATP-binding cassette (ABC) transporter family, is involved in the efflux of Dox-conjugated block copolymers [14]. ABCB1, also known as MDR-1 or P-gp, is an efflux pump for various drugs. In this study, we assessed the involvement of other types of ABC transporters and exocytosis in the extracellular efflux of polymers from HeLa cells. The knockdown of various ABC transporters (ABCA1, ABCB1, ABCC1, and ABCG1) caused the intracellular amounts of all polymers at 24 h after micelle addition to increase when ABCB1 expression was suppressed, but not when ABCA1, ABCC1, or ABCG1 expression was



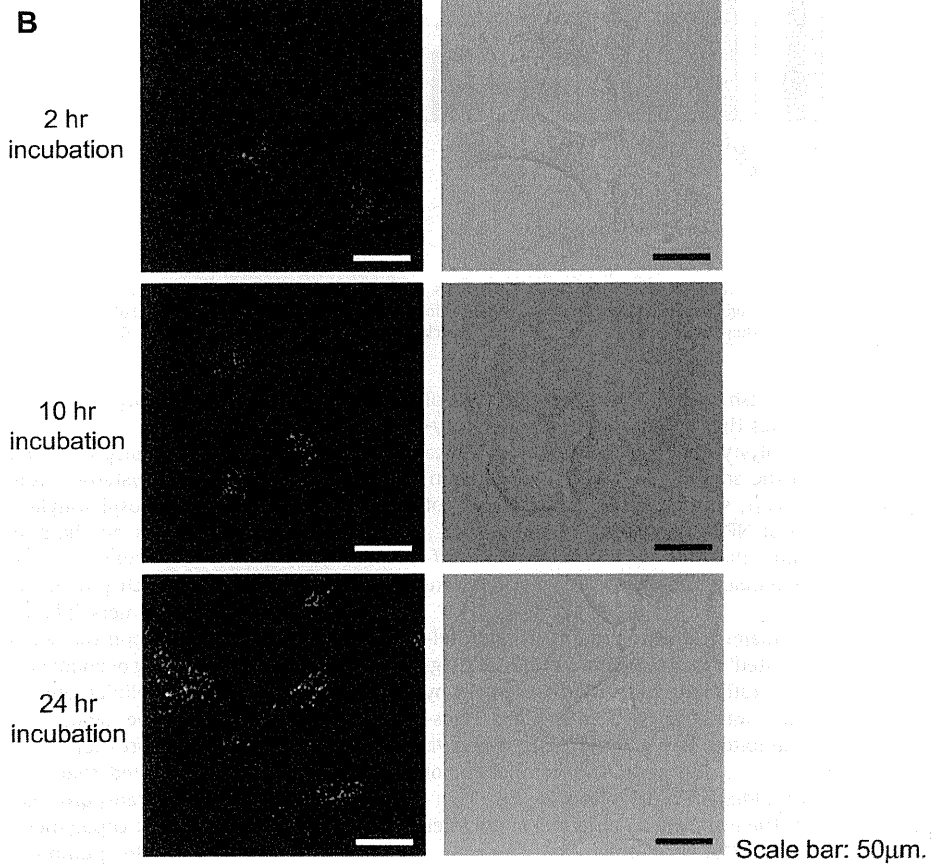
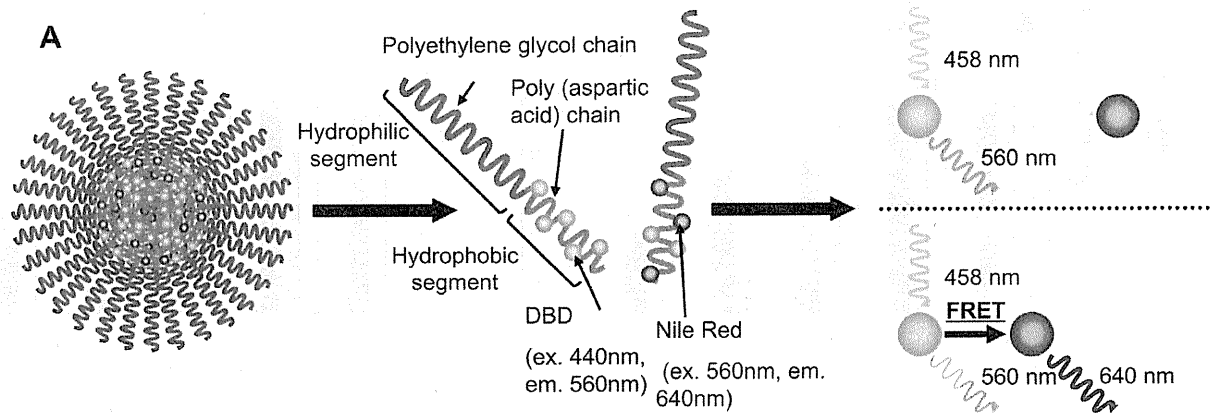


**Fig. 3.** (A) Schematic of FRET micelles used to investigate the structural integrity of micelles in HeLa cells. The fluorescent intensity of the donor, DBD (excitation 440 nm; emission 580 nm), enhanced the effective excitation of the acceptor, Nile Red (excitation 580 nm; emission 640 nm). (B) Confocal images of the fluorescent spectral shift that corresponds to the dissociation of FRET micelles. Cells were exposed to 50 µg/mL FRET micelles in culture medium. Two hours after the addition of micelles, the cells were washed and kept in medium without micelles; they were then subjected to confocal imaging at 2, 10, and 24 h after the addition of the micelles. Scale bars = 50 µm.

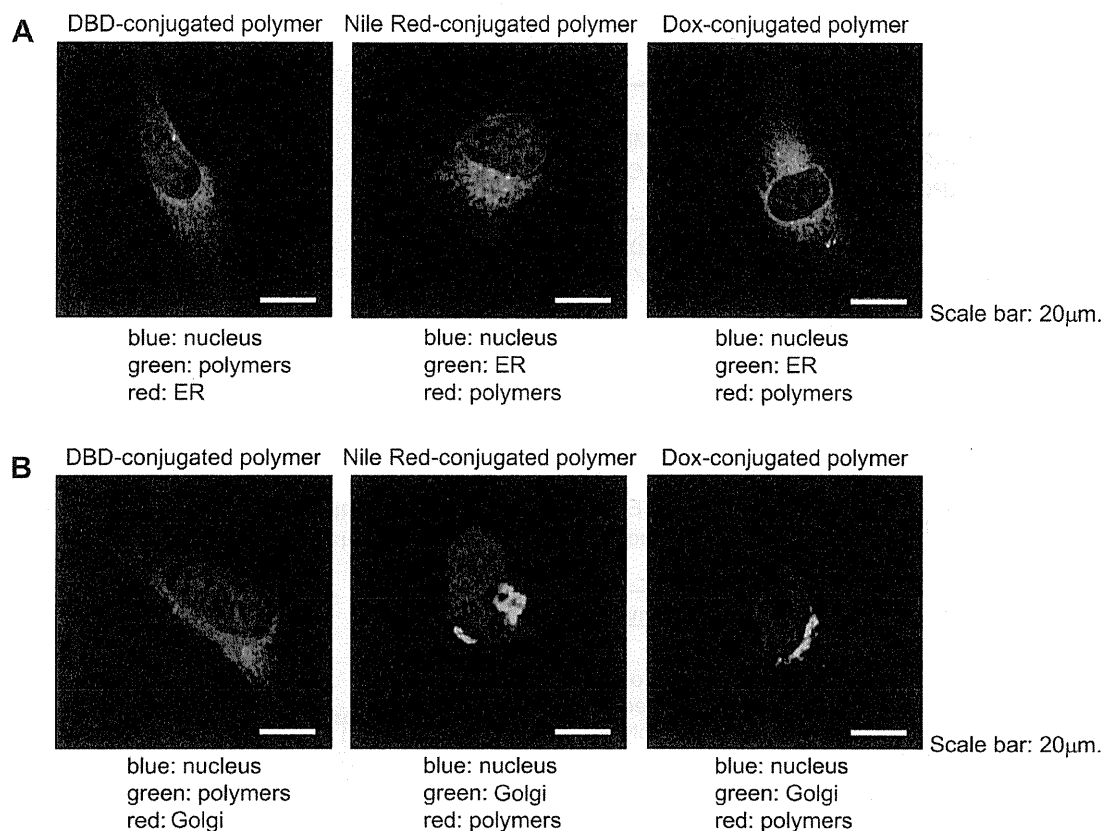


**Fig. 4.** Confocal images showing the intracellular localization of polymers at 24 h after the addition of micelles to HeLa cells. ER (A) and Golgi apparatus (B) were labeled with ER-Tracker and BODIPY-ceramide, respectively. Scale bars = 20 μm.

suppressed (Fig. 7A). On the other hand, the suppression of ABCB1 transporter expression did not lead to an increase in the intracellular amounts of dextran, polystyrene nanoparticle, or silica nanoparticle (Supplementary Fig. 5B).

With respect to exocytosis, the intracellular amounts of the polymers were also unaffected by the presence of snap-25, a known exocytosis-related protein (Fig. 7B).

### 3.7. The transport of polymers by ABCB1

The possibility remained that efflux only occurred for fluorescent compounds that were no longer conjugated to the polymers. Therefore, to further confirm the involvement of the ABCB1 transporter in the efflux of block copolymers, we used membranes expressing ABCB1. ATP-dependent transport increased at higher polymer concentrations for DBD-, Nile Red-, and Dox-conjugated polymers (Fig. 8A). All of the block polymers were transported through the membranes that expressed ABCB1, but were not transported through control membranes that lacked ABCB1 (Fig. 8B). To examine whether ABCB1 recognizes the conjugated fluorescent compounds or the polymer itself, we also examined the ATP-dependent transport of free DBD, Nile Red, and Dox and found that intravesicular uptake of DBD and Nile Red did not occur (Fig. 8C). Transport was observed for Dox, which is a well-known substrate of ABCB1. These findings indicate that the intravesicular fluorescence observed in our study and extracellular efflux observed in Fig. 7A did not stem from free fluorescent compounds, but rather from the fluorescent compounds conjugated to the polymers. Therefore, ABCB1 recognizes the block copolymer.

## 4. Discussion

The aim of this study was to elucidate the molecular mechanisms involved in the intracellular trafficking and extracellular efflux of block copolymer micelles and their components. In this study, we used block copolymer micelles conjugated with the fluorescent compounds Dox, DBD, and Nile Red.

The intracellular uptake of micelles was inhibited in the presence of chlorpromazine in HeLa cells (Fig. 2), suggesting that all micelles are taken up into the cells via clathrin-mediated endocytosis. However, caveolae-mediated endocytosis was also observed to some extent in all micelles as the incubation time progressed. The P85 amphiphilic triblock copolymer, which is composed of poly(ethylene oxide) (PEO) and poly(propylene oxide) (PPO), is internalized predominantly through caveolae-mediated endocytosis, although in the micelle form P85 is internalized exclusively through clathrin-mediated endocytosis [12,38].

FRET is a technique that has been used recently to measure the stability and dissociation of drug delivery system carriers and the release of encapsulated drugs. By using FRET micelles, we determined that micelle dissociation occurs within endosomes or lysosomes after internalization via endocytosis. This result indicates that the release of encapsulated drugs from these micelles will occur in endosomes or lysosomes.

We also investigated the molecular mechanisms involved in the intracellular trafficking of the block copolymers. When NPC1 expression was inhibited, the intracellular amounts of polymer increased (Fig. 5B). Confocal microscopy revealed that the knock-down of NPC1 expression suppressed the transport of the polymers

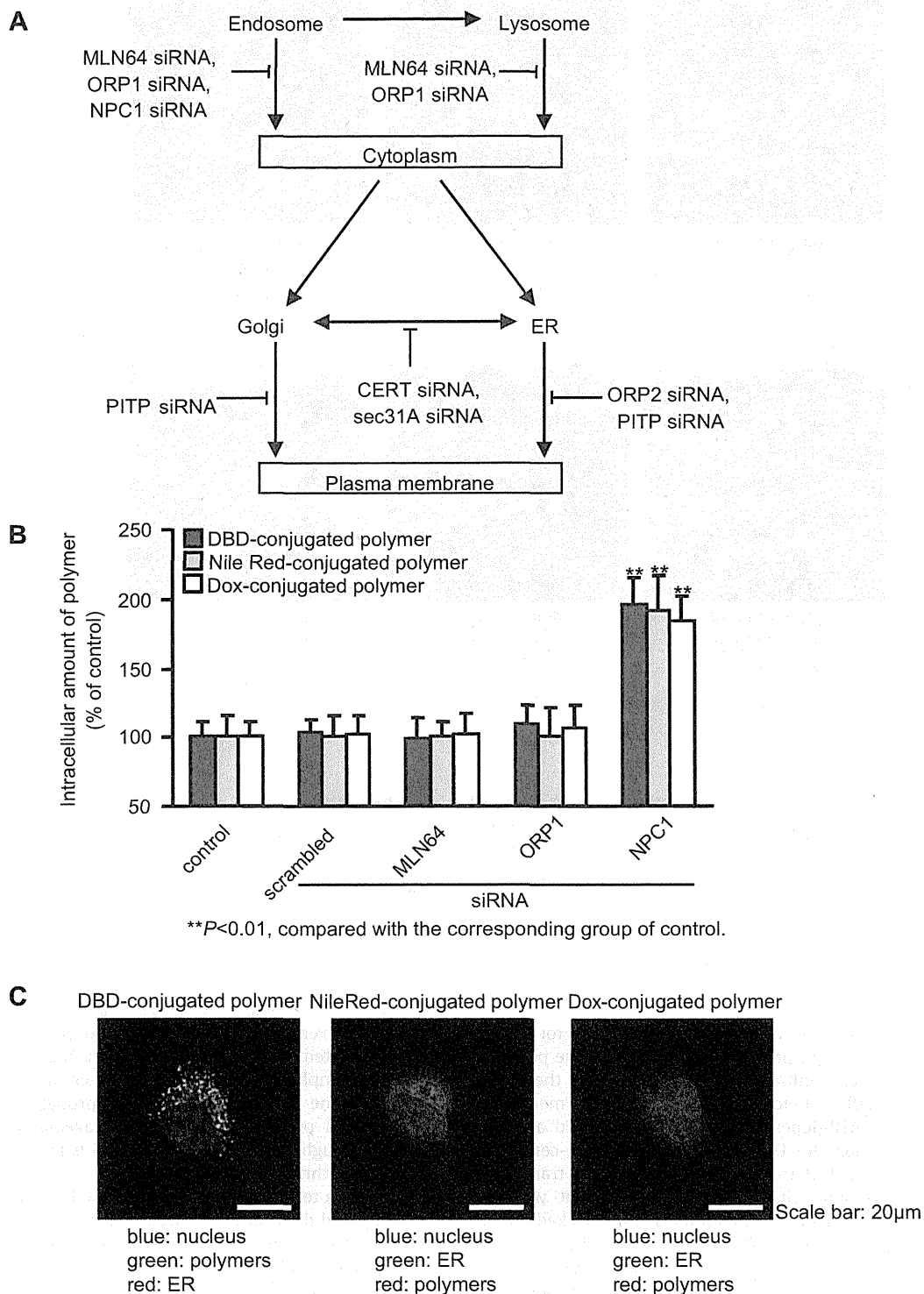
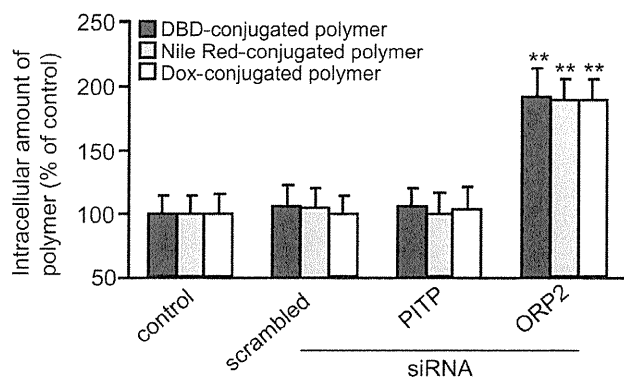
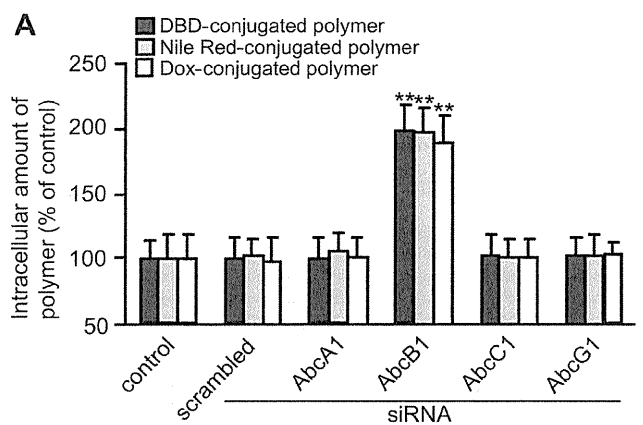


**Fig. 5.** (A) Intracellular components and typical lipid transport proteins. The expression of these proteins was suppressed by siRNA. (B) Intracellular amounts of polymers under suppressing conditions for each protein (MLN64, ORP1, and NPC1) at 24 h after the addition of micelles to HeLa cells. Cells were transfected with siRNAs against the targeted proteins by using Lipofectamine RNAiMAX according to the recommended protocols.  $**P < 0.01$  compared with the corresponding control group. Each value represents the mean  $\pm$  SD ( $n = 6$ ). (C) Confocal images showing the intracellular localization of micelles under suppressing conditions for NPC1 at 24 h after the addition of micelles to HeLa cells. The ER was labeled with ER-Tracker. Scale bars = 20  $\mu$ m.



\*\* $P < 0.01$ , compared with the corresponding group of control.

**Fig. 6.** Effect of siRNA-induced knockdown of ORP2 and PITP on the intracellular amounts of polymers. The figure shows the intracellular amounts of polymer under suppressing conditions for ORP2 or PITP at 24 h after the addition of micelles to HeLa cells. \*\* $P < 0.01$  compared with the corresponding control group. Each value represents the mean  $\pm$  SD ( $n = 6$ ).



\*\* $P < 0.01$ , compared with the corresponding group of control.

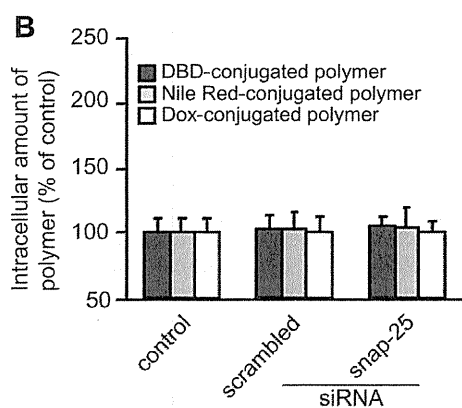


**Fig. 7.** (A) Effect of siRNA-induced knockdown of ABC transporters on the intracellular amounts of polymers. The figure shows the intracellular amounts of polymer under suppressing conditions for various ABC transporters (ABCA1, ABCB1, ABCC1, and ABCG1) at 24 h after the addition of micelles to HeLa cells. (B) The intracellular amounts of polymers under suppressing conditions for snap-25 at 24 h after the addition of micelles to HeLa cells. The cells were transfected with siRNAs against the targeted proteins by using Lipofectamine RNAiMAX according to the recommended protocols. \*\* $P < 0.01$  compared with the corresponding control group. Each value represents the mean  $\pm$  SD ( $n = 6$ ).

from endosomes or lysosomes to the ER (Fig. 5C). Our results also suggest that ER-to-Golgi transport is not involved in the intracellular trafficking of block copolymers (Supplementary Fig. 4). This is consistent with our observation that the polymer did not localize to the Golgi apparatus (Fig. 4B). Taken with the results of the FRET micelle experiments, the confocal images suggest that the micelles used in this study dissociate into their individual components in late endosomes, and after dissociation, the polymers are extracted by NPC1 from the endosomes and transferred to the ER (Fig. 9). We confirmed that 4-phenyl-1-butanol, which was conjugated to the polymers to increase their hydrophobicity, was not released from the polymers under the experimental conditions used (Supplementary Fig. 6). Therefore, the release of the conjugated compounds is not the driving force for the dissociation of the micelles in late endosomes or lysosomes. The driving force for this dissociation remains to be elucidated.

NPC1 facilitates the trafficking of low density lipoprotein-derived cholesterol from the late endosome to various destinations such as the plasma membrane, the trans-golgi network, and the ER [39]. Similarly, it appears that NPC1 enhances the trafficking of dissociated polymers from late endosomes to the ER. Although direct trafficking from the late endosome to the plasma membrane is a possibility [40], such trafficking would probably represent a small proportion of the total trafficking given our finding that the inhibition of trafficking from the ER to the plasma membrane led to the retention of most of the intracellular block copolymers. Sahay G et al. reported that NPC1 is an important regulator of the major recycling pathways of lipid nanoparticle-delivered siRNA, although they did not investigate the trafficking of the carrier components, but rather tracked the labeled siRNA. They demonstrated that NPC1-deficient cells show enhanced cellular retention of lipid nanoparticles inside late endosomes because of the decrease in motility of late endosomes [40,41]. These findings indicate that NPC1 is a key factor in determining the fate of block copolymers.

Although some of the block copolymers might have been retained in vesicles and transferred to lysosomes, the dissociated polymers in the late endosomes were transported to the ER. Our results also indicate that encapsulated drugs could be released from these micellar carriers in late endosomes and diffuse into the cytoplasm at this stage, demonstrating that such micelles are suitable for the intracellular delivery of degradable compounds, such as nucleic acids or proteins, and can minimize the degradation of these compounds in lysosomes. We also investigated the extracellular efflux mechanisms of block copolymers. As shown in Fig. 6, the transport of block copolymers to the cell membrane was affected by ORP2 (Fig. 9). ORP2 is involved in the vesicle-independent intermembrane transport of lipophilic compounds [32–34], and the ER possesses closed sites at the cell membrane [42]. Hao et al. reported that endogenous cholesterol is transported to cell membranes via the ER [43]. Therefore, the block copolymers in the present study might also be transferred to the cell membrane via these closed sites (Fig. 9). Following the transfer to the plasma membrane, efflux of the block copolymers mainly occurred via ABCB1 but not ABCA1, ABCC1, or ABCG1 (Figs. 7 and 9). SNARE proteins, such as snap-25, control the extracellular efflux of various compounds, including proteins and lipids, via exocytosis [44,45]. Although the expression levels of SNARE-related proteins are high in specific cancer cells, including HeLa cells [44–46], exocytosis did not appear to be involved in the extracellular efflux of block copolymers from HeLa cells (Fig. 7B), and the block copolymers used in our studies were effluxed only through the ABCB1.

Lastly, we investigated the molecular mechanism of block copolymer efflux through transporters by using vesicles that expressed ABCB1. All of the polymers, regardless of PEG chain length, polymerization degree of P(Asp), or fluorescent compound,

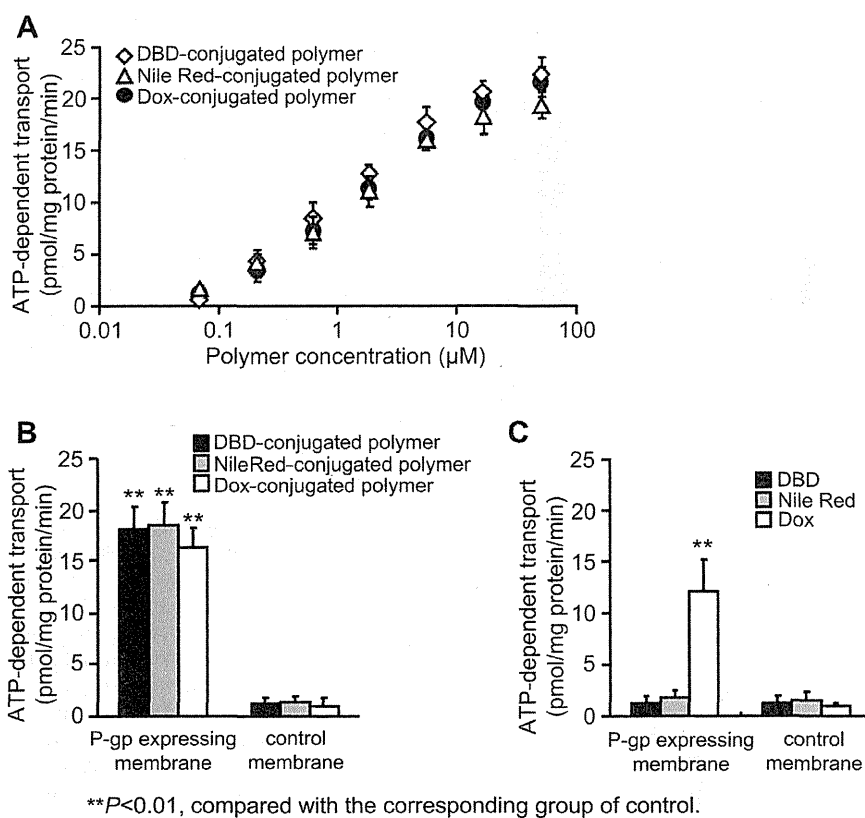


**Fig. 8.** ATP-dependent uptake of polymers by ABCB1-expressing membrane vesicles. Suspensions of membranes expressing ABCB1, or control membranes that did not express ABCB1 (50  $\mu$ L each) were plated on a 96-well plate. (A) Increasing polymer transport with increasing polymer concentration. Samples at the indicated concentration were added to each well, respectively, and the plates were incubated at 37  $^{\circ}$ C for 5 min. After washing by centrifugation, the fluorescence intensity of the transported polymers was measured. Each value represents the mean  $\pm$  SD ( $n = 6$ ). (B) Transport of fluorescent polymers into vesicles expressing ABCB1.  $**P < 0.01$ , compared with the corresponding control group. Each value represents the mean  $\pm$  SD ( $n = 6$ ). (C) Transport of free fluorescent compounds into vesicles expressing ABCB1.  $**P < 0.01$ , compared with the corresponding control group. Each value represents the mean  $\pm$  SD ( $n = 6$ ).

underwent similar transport into the vesicles expressing ABCB1 (Fig. 8B). Free DBD and Nile Red were not, however, transported through ABCB1 (Fig. 8C), indicating that the observed changes in fluorescence did in fact correspond to the transport of the polymers and not to that of dissociated Dox, DBD, or Nile Red. This result indicates that the block copolymers themselves are crucial to their transport by ABCB1, and that the conjugated fluorescent compound is not recognized by ABCB1. The ABCB1 transporter plays a critical role in drug clearance, including urinary excretion in the kidneys, and biliary excretion in the liver [47]. We are currently investigating the role of the ABCB1 transporter in the dynamics and clearance of the polymer and encapsulated drugs *in vivo*.

All of the micelles used in this study showed the same intracellular trafficking and the same proteins were involved in that trafficking, independent of PEG chain length, polymerization degree of P(Asp), and the hydrophobic moiety introduced into the core segment within the range investigated. To determine whether the intracellular trafficking and the molecular mechanism were specific to the block copolymer we used, we tested the more hydrophilic polymer dextran. Dextran is a macropinocytosis marker, and in fact its internalization was inhibited by the macropinocytosis inhibitor EIPA (Supplementary Fig. 7). Because it is possible that macropinosomes directly fuse with NPC1-positive late endosomes [48], dextran can be recycled to the extracellular milieu by NPC1. However, NPC1 was not involved in the trafficking of dextran from the late endosome (Supplementary Fig. 3). Moreover, knockdown of ORP2 and ABCB1 expression, which is involved in block copolymer trafficking, was not involved in the intracellular

trafficking of dextran (Supplementary Fig. 5). We also tested a hydrophobic nanoparticle (a polystyrene nanoparticle) and a hydrophilic nanoparticle (a silica nanoparticle) with respect to their intracellular trafficking. The internalization of these nanoparticles was mediated by both clathrin-mediated endocytosis and caveolae-mediated endocytosis (Supplementary Fig. 7) similarly to the block copolymers and micelles we used. However, NPC1, ORP2, and ABCB1 were not involved in the intracellular trafficking of these nanoparticles (Supplementary Figs. 3 and 5). Yet, the efflux of dextran, polystyrene nanoparticles, and silica nanoparticles is controlled by the exocytosis protein snap-25 (Supplementary Fig. 8). Thus, the findings described in this report regarding the intracellular fate of the block copolymers and the intrinsic proteins involved in their trafficking are specific to these block copolymers. From a safety standpoint, further studies are needed to elucidate the physicochemical properties of block copolymers that determine their intracellular trafficking and fate so that we might be able to predict the potential for accumulation of newly developed block copolymers inside cells and/or their efflux from cells. It will also be necessary to elucidate the intracellular trafficking and fate of block copolymers in different cell types.

## 5. Conclusions

We have characterized here the intracellular trafficking and fate of different block copolymer micelles and their dissociated polymers, from intracellular uptake to extracellular efflux. In addition, we identified three proteins that are involved in the intracellular

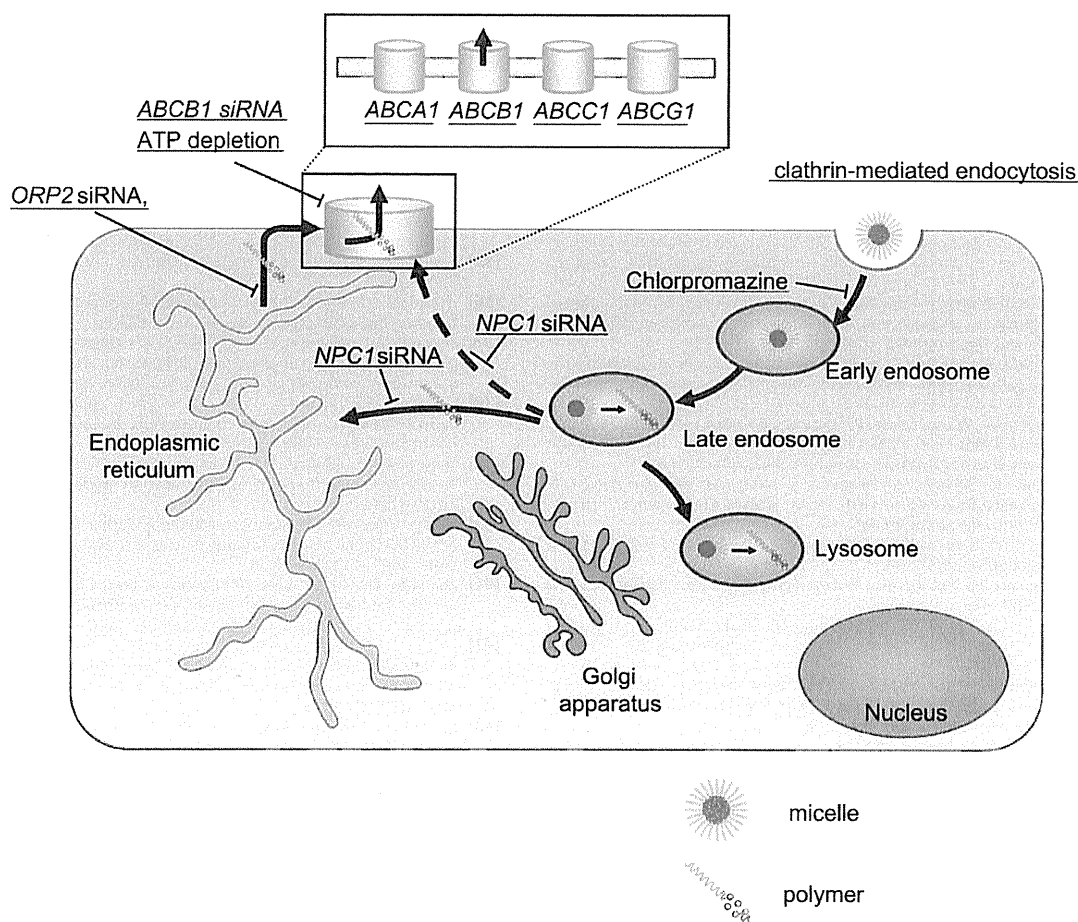


Fig. 9. Predicted mechanism of intracellular trafficking of micelles and polymers used in this study.

trafficking of these polymers: NPC1, ORP2, and ABCB1 (Fig. 9). By using FRET micelles, we showed that the dissociation of the micelles occurs mainly in late endosomes and that NPC1 seems to have a key role in the dissociation of micelles and in the intermembrane transfer of the block copolymers.

Exocytosis is well-known efflux route for nanoparticles internalized by endocytosis. Our study has elucidated a unique trafficking and efflux route for the components of block copolymer micelles in which NPC1 and ORP2 play essential role in the transfer of the block copolymers to their efflux via the transporter ABCB1. This route can prevent the accumulation of components inside the cells after intracellular uptake via endocytosis. Such knowledge may help improve the therapeutic efficacy and minimize the safety risks of block copolymer micelles.

#### Acknowledgments

This work was supported in part by Public-Private Sector Joint Research on Publicly Essential Drugs from the Japan Health Sciences Foundation, by Health and Labour Sciences Research Grants from the Ministry of Health, Labour and Welfare of Japan, and by JSPS KAKENHI Grant number 24590070. We thank Nippon Kayaku Co. Ltd for providing the block copolymers.

#### Appendix A. Supplementary data

Supplementary data related to this article can be found at <http://dx.doi.org/10.1016/j.biomaterials.2013.11.027>.

#### References

- [1] Barenholz Y. Doxil<sup>®</sup> – the first FDA-approved nano-drug: lessons learned. *J Control Release* 2012;160:117–34.
- [2] Duncan R, Gaspar R. Nanomedicine(s) under the microscope. *Mol Pharm* 2011;8:2101–41.
- [3] Ferrari M. Cancer nanotechnology: opportunities and challenges. *Nat Rev Cancer* 2005;5:161–71.
- [4] Kataoka K, Kwon GS, Yokoyama M, Okano T, Sakurai Y. Block copolymer micelles as vehicles for drug delivery. *J Control Release* 1993;24:119–32.
- [5] Nishiyama N, Kataoka K. Current state, achievements, and future prospects of polymeric micelles as nanocarriers for drug and gene delivery. *Pharmacol Ther* 2006;112:630–48.
- [6] Torchilin VP. PEG-based micelles as carriers of contrast agents for different imaging modalities. *Adv Drug Deliv Rev* 2002;54:235–52.
- [7] Kabanov A, Zhu J, Alakhov V. Pluronic block copolymers for gene delivery. *Adv Genet* 2005;53:231–61.
- [8] Uchino H, Matsumura Y, Negishi T, Koizumi F, Hayashi T, Honda T, et al. Cisplatin-incorporating polymeric micelles (NC-6004) can reduce nephrotoxicity and neurotoxicity of cisplatin in rats. *Br J Cancer* 2005;93:678–87.
- [9] Hamaguchi T, Matsumura Y, Suzuki M, Shimizu K, Goda K, Nakamura I, et al. NK105, a paclitaxel-incorporating micellar nanoparticle formulation, can extend in vivo antitumor activity and reduce the neurotoxicity of paclitaxel. *Br J Cancer* 2005;92:1240–6.
- [10] Koizumi F, Kitagawa M, Negishi T, Onda T, Matsumoto S, Hamaguchi T, et al. Novel SN-38-incorporating polymeric micelles, NK012, eradicate vascular endothelial growth factor-secreting bulky tumors. *Cancer Res* 2006;15(66):10048–56.
- [11] Murakami M, Cabral H, Matsumoto Y, Wu S, Kano MR, Yamori T, et al. Improving drug potency and efficacy by nanocarrier-mediated subcellular targeting. *Sci Transl Med* 2011;3:64ra2.
- [12] Sahay G, Patrakova EV, Kabanov AV. Different internalization pathways of polymeric micelles and unimers and their effects on vesicular transport. *Bioconjug Chem* 2008;19:2023–9.
- [13] Hatakeyama H, Akita H, Harashina H. A multifunctional envelope type nano device (MEND) for gene delivery to tumours based on the EPR effect.

- a strategy for overcoming the PEG dilemma. *Adv Drug Deliv Rev* 2011;63:152–60.
- [14] Sakai-Kato K, Ishikura K, Oshima Y, Tada M, Suzuki T, Ishii-Watabe A, et al. Evaluation of intracellular trafficking and clearance from HeLa cells of doxorubicin-bound block copolymers. *Int J Pharm* 2012;423:401–9.
- [15] Nakanishi T, Fukushima S, Okamoto K, Suzuki M, Matsumura Y, Yokoyama M, et al. Development of the polymer micelle carrier system for doxorubicin. *J Control Release* 2001;74:295–302.
- [16] Rejman J, Bragonzi A, Conese M. Role of clathrin- and caveolae-mediated endocytosis in gene transfer mediated by lipo- and polyplexes. *Mol Ther* 2005;12:468–74.
- [17] Perez AP, Cosaka ML, Romero EL, Morilla M. Uptake and intracellular traffic of siRNA dendriplexes in glioblastoma cells and macrophages. *Int J Nanomed* 2011;6:2715–28.
- [18] Tomás M, Martínez-Alonso E, Ballesta J, Martínez-Menárguez JA. Regulation of ER-Golgi intermediate compartment tubulation and mobility by COPI coats, motor proteins and microtubules. *Traffic* 2010;11:616–25.
- [19] Uematsu K, Seki N, Seto T, Ise C, Tsukamoto H, Mikami I, et al. Targeting the Wnt signaling pathway with disbevelled and cisplatin synergistically suppresses mesothelioma cell growth. *Anticancer Res* 2007;27:4239–42.
- [20] Chen H, Kim S, He W, Wang H, Low PS, Park K, et al. Fast release of lipophilic agents from circulating PEG-PDIIA micelles revealed by in vivo forster resonance energy transfer imaging. *Langmuir* 2008;24:5213–7.
- [21] Müller T, Rachel R, Besheer A, Uezguen S, Weigand M, Goeferich A. Comparative investigations on in vitro serum stability of polymeric micelle formulations. *Pharm Res* 2012;29:448–59.
- [22] Ioannou YA. Multidrug permeases and subcellular cholesterol transport. *Nat Rev Mol Cell Biol* 2001;2:657–68.
- [23] Minceo C, Anderson RG. Pinocytosis. Robert Feulgen Lecture. *Histochem Cell Biol* 2001;116:109–18.
- [24] Hólttä-Vuori M, Alpy F, Tanhuaupää K, Jokitalo E, Mutka AL, Ikonen E. MLN64 is involved in actin-mediated dynamics of late endocytic organelles. *Mol Biol Cell* 2005;16:3873–86.
- [25] Xu Y, Liu Y, Ridgway ND, McMaster CR. Novel members of the human oxysterol-binding protein family bind phospholipids and regulate vesicle transport. *J Biol Chem* 2001;276:18407–14.
- [26] Ikonen E. Cellular cholesterol trafficking and compartmentalization. *Nat Rev Mol Cell Biol* 2008;9:125–38.
- [27] Koivusalo M, Jansen M, Sommerharju P, Ikonen E. Endocytic trafficking of sphingomyelin depends on its acyl chain length. *Mol Biol Cell* 2007;18:5113–23.
- [28] Hanada K, Kumagai K, Yasuda S, Miura Y, Kawano M, Fukasawa M, et al. Molecular machinery for non-vesicular trafficking of ceramide. *Nature* 2003;426:803–9.
- [29] Hanada K, Kumagai K, Tomishige N, Yamaji T. CERT-mediated trafficking of ceramide. *Biochim Biophys Acta* 2009;1791:684–91.
- [30] Sato K, Nakano A. Mechanisms of COPII vesicle formation and protein sorting. *FEBS Lett* 2007;581:2076–82.
- [31] Townley AK, Feng Y, Schmidt K, Carter DA, Porter R, Verkade P, et al. Efficient coupling of Sec23–Sec24 to Sec13–Sec31 drives COPII-dependent collagen secretion and is essential for normal craniofacial development. *J Cell Sci* 2008;121:3025–34.
- [32] Laitinen S, Lehto M, Lehtonen S, Hyvärinen K, Heimo S, Lehtonen E, et al. ORP2, a homolog of oxysterol binding protein, regulates cellular cholesterol metabolism. *J Lipid Res* 2002;43:245–55.
- [33] Hyytiäinen R, Laitinen S, Käkälä R, Tanhuaupää K, Lusa S, Ehnholm C, et al. Overexpression of OSBP-related protein 2 (ORP2) induces changes in cellular cholesterol metabolism and enhances endocytosis. *Biochem J* 2005;390:273–83.
- [34] Hyytiäinen R, Suchanek M, Spandt J, Bäck N, Thiele C, Ollikonen VM. OSBP-related protein 2 is a sterol receptor on lipid droplets that regulates the metabolism of neutral lipids. *J Lipid Res* 2009;50:1305–15.
- [35] Wirtz KW. Phospholipid transfer proteins revisited. *Biochem J* 1997;324:353–60.
- [36] Hsuan J, Cockcroft S. The PTP family of phosphatidylinositol transfer proteins. *Genome Biol* 2001;2: reviews 3011.1–3011.8.
- [37] Séguin B, Allen-Baume V, Cockcroft S. Phosphatidylinositol transfer protein beta displays minimal sphingomyelin transfer activity and is not required for biosynthesis and trafficking of sphingomyelin. *Biochem J* 2002;366:23–34.
- [38] Batrakova EV, Kabanov AV. Pluronic block copolymers: evolution of drug delivery concept from inert nanocarriers to biological response modifiers. *J Control Release* 2008;130:98–106.
- [39] Sugii S, Lin S, Ohgami N, Ohashi M, Chang CC, Chang TY. Roles of endogenously synthesized sterols in the endocytic pathway. *J Biol Chem* 2006;281:23191–206.
- [40] Sahay G, Querbes W, Alabi C, Eltoukhy A, Sarkar S, Zareno C, et al. Efficiency of siRNA delivery by lipid nanoparticles is limited by endocytic recycling. *Nat Biotechnol* 2013;31:653–8.
- [41] Zhang M, Dwyer NK, Love DC, Cooney A, Comly M, Neufeld E, et al. Cessation of rapid late endosomal tubulovesicular trafficking in Niemann-Pick type C1 disease. *Proc Natl Acad Sci U S A* 2001;98:4466–71.
- [42] Pichler H, Gaigg B, Hrastnik C, Achleitner G, Kohlwein SD, Zellnig G, et al. A subfraction of the yeast endoplasmic reticulum associates with the plasma membrane and has a high capacity to synthesize lipids. *Eur J Biochem* 2001;268:2351–61.
- [43] Hao M, Lin SX, Karylowski OJ, Wüstner D, McGraw TE, Maxfield FR. Vesicular and non-vesicular sterol transport in living cells. The endocytic recycling compartment is a major sterol storage organelle. *J Biol Chem* 2002;277:609–17.
- [44] Néméz-Gaillard E, Bosshard A, Regazzi R, Bernard C, Cuber JC, Takahashi M, et al. Expression of SNARE proteins in enteroendocrine cell lines and functional role of tetanus toxin-sensitive proteins in cholecystokinin release. *FEBS Lett* 1998;425:66–70.
- [45] Bonifacino JS, Glick BS. The mechanisms of vesicle budding and fusion. *Cell* 2004;116:153–66.
- [46] Okayama M, Arakawa T, Mizoguchi I, Tajima Y, Takuma T. SNAP-23 is not essential for constitutive exocytosis in HeLa cells. *FEBS Lett* 2007;581:4583–8.
- [47] Tanigawara Y. Role of P-glycoprotein in drug disposition. *Ther Drug Monit* 2000;22:137–40.
- [48] Kerr MC, Teasdale RD. Defining macropinocytosis. *Traffic* 2009;10:364–71.



## High-performance liquid chromatography separation of monoclonal IgG2 isoforms on a column packed with nonporous particles

Cite this: *Anal. Methods*, 2013, 5, 5899Received 25th July 2013  
Accepted 9th September 2013

DOI: 10.1039/c3ay41249k

www.rsc.org/methods

Kumiko Sakai-Kato,<sup>\*a</sup> Kunie Nanjo,<sup>a</sup> Teruhide Yamaguchi,<sup>b</sup> Haruhiro Okuda<sup>b</sup> and Toru Kawanishi<sup>b</sup>

The IgG2 subclass of antibodies has emerged as an attractive therapeutic framework. However, a method for sufficiently separating the three IgG2 disulfide isoforms has not been developed. Here, we report a method for efficient separation of monoclonal IgG2 isoforms by means of high-performance liquid chromatography on a column packed with 2  $\mu\text{m}$  nonporous ODS silica particles. Under optimized conditions, the isoforms were separated with high resolution because mass transfer resistance in the stationary phase was reduced by the use of the small, nonporous particles. The number of separated peaks was more than twice that reported previously. The run-to-run repeatability of the IgG2 separation pattern was satisfactory, and the day-to-day repeatability of the retention time of the main peak was good (relative standard deviation 0.9%). The separation pattern can be expected to be useful for monitoring quality consistency of therapeutic antibodies.

## 1. Introduction

Human monoclonal antibodies, including three of the four subclasses of immunoglobulin G (IgG1, IgG2, and IgG4), have been widely used as therapeutic drugs. Although members of the IgG1 subclass are the most widely used therapeutic antibodies, the IgG2 subclass has emerged as an attractive therapeutic framework in situations in which effector functions are undesirable or unnecessary for therapeutic activity;<sup>1,2</sup> the effector functions of IgGs depend on their affinity for Fc $\gamma$  receptors, which decreases in the order IgG1, IgG3 > IgG2, IgG4.<sup>3,4</sup> The most characteristic structural differences between the four subclasses are the numbers and positions of disulfide bonds linking Cys residues in the hinge regions:<sup>5</sup> IgG1 and IgG4 have two, whereas IgG2 has four (Fig. 1).

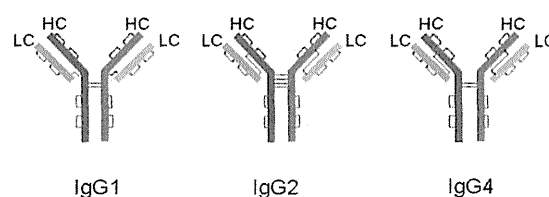


Fig. 1 Schematic showing human IgG subtypes, with disulfide links.

IgG2 antibodies were recently shown to exist in three disulfide-mediated structural isoforms.<sup>6–8</sup> The effect of structural heterogeneity on antibody function has attracted much attention,<sup>7</sup> and interconversion between the isoforms *in vivo* and their pharmacokinetics have also been studied.<sup>8</sup> In addition to structural heterogeneity, IgGs also show heterogeneity in various other properties, such as charge. Gaining a comprehensive understanding of the structure and stability of the isoforms is important for quality control, and with this goal in mind, separation of the isoforms by means of high-performance liquid chromatography (HPLC) has been studied.<sup>9–11</sup> However, although resolution has been improved, separation of the IgG2 isoforms remains insufficient. Here, we report the development of a method for highly efficient separation of IgG2 isoforms by means of HPLC on a column packed with 2  $\mu\text{m}$  nonporous ODS silica particles.

## 2. Experimental

### 2.1 Materials

The following commercially available monoclonal IgGs (IgG1, IgG2, and IgG4 subclasses) were purchased from reagent distributors: infliximab (hereafter referred to as IgG1#1), trastuzumab (IgG1#2), panitumumab (IgG2#1), denosumab (IgG2#2), and natalizumab (IgG4#1). Trifluoroacetic acid (TFA), acetonitrile, and ethylenediaminetetraacetic acid were purchased from Wako Pure Chemical Industries (Osaka, Japan). Other reagents were obtained from Sigma-Aldrich Co. (St. Louis, MO, USA).

<sup>a</sup>Division of Drugs, National Institute of Health Sciences, 1-18-1 Kamiyoga, Setagaya-ku, Tokyo 158-8501, Japan. E-mail: kumikato@nihs.go.jp; Fax: +81-3-3700-9662; Tel: +81-3-3700-9662

<sup>b</sup>National Institute of Health Sciences, 1-18-1 Kamiyoga, Setagaya-ku, Tokyo 158-8501, Japan

## 2.2 HPLC conditions

IgG2 isoforms were separated on a Hitachi LaChromUltra HPLC system equipped with an L-2160U pump, an L-2200U automated sample injector, an L-2300 thermostatted column compartment, and an L-2485U fluorescence detector (Hitachi, Tokyo, Japan).

IgG2 isoforms were separated on a Presto FF-C18 column (250 × 4.6 mm; particle size, 2 μm; Imtakt Corp., Kyoto, Japan) with mixtures of water containing 0.1% TFA (mobile phase A) and acetonitrile containing 0.1% TFA (mobile phase B) at a flow rate of 400 μL min<sup>-1</sup>. Samples were injected under loading conditions of 31, 32, 33, or 34% B, and the proportion of B was increased to 44, 43, 42, or 41% B, respectively, by means of a linear elution gradient starting at 0 min and ending at 60 min. The column was then flushed for 5 min with 95% B. The column temperature was maintained at 85 °C, the detector was operated at 220 nm, and the column pressure was approximately 15 MPa.

## 2.3 Reduction and alkylation of IgGs

IgG samples were diluted to 1 mg mL<sup>-1</sup> in a pH 7.5 buffer containing 7.5 M guanidine hydrochloride, 0.1 M Tris-HCl, and 1 mM ethylenediaminetetraacetic acid to a final volume of 0.5 mL. Dithiothreitol (final concentration 5 mM) was added to the samples, which were then incubated at 37 °C for 35 min. After the addition of iodoacetic acid (final concentration 13 mM), the samples were cooled to room temperature and then incubated at room temperature in the dark for 1 hour.<sup>10</sup>

## 3. Results and discussion

Incomplete separation of intact IgG2 isoforms by means of reversed-phase HPLC on columns packed with 5 μm porous or spherically porous particles has been reported.<sup>10,11</sup> In this study, we improved the separation by using a stationary phase packed with smaller (2 μm), nonporous particles.

The effect of stationary phase particle characteristics on plate height ( $H$ ) can be determined with the van Deemter equation:

$$H = A + \frac{B}{u} + Cu \quad (1)$$

where  $H$  is the plate height,  $u$  is the linear velocity of the mobile phase, and  $A$ ,  $B$ , and  $C$  are constants that account for contributions to band broadening from eddy diffusion, longitudinal diffusion, and resistance to mass transfer of analytes, respectively. In the case of macromolecules, the effect of longitudinal diffusion (the  $B$  term) is generally negligible. The major difference between porous and nonporous particles is that for porous particles, resistance to mass transfer (the  $C$  term) is appreciable, owing to stagnation of the mobile phase in the pores. The Horvath-Lin equation describes the contribution of resistance to mass transfer ( $C_{\text{stag}}$ ) for unretained solutes:<sup>12</sup>

$$C_{\text{stag}} = \frac{\theta k_0 d_p^2}{30D_m(1 + k_0)^2} \quad (2)$$

where  $\theta$  is the tortuosity factor for porous particles,  $k_0$  is the ratio of the intraparticle void space to the interstitial void space in the column,  $D_m$  is the diffusion coefficient of the solute in the mobile phase, and  $d_p$  is the particle diameter. The contribution of  $C_{\text{stag}}$  becomes appreciable when analytes with relatively high molecular weights (relatively small  $D_m$  values) are separated. An increase in molecular weight results in a decrease in the diffusion coefficient and an increase in the mass transfer resistance. Therefore, the diffusion of large molecules in the pores makes a large contribution to the mass transfer resistance. These facts suggest that nonporous particles have a substantial advantage over porous particles for efficient separation of large molecules.<sup>13</sup> Nonporous columns have previously been reported to afford higher rates of peptide recovery than porous columns.<sup>14</sup> Furthermore, decreasing the particle size also contributes to decreases in the  $A$  and  $C$  terms of eqn (1), which in turn lead to a reduction in  $H$  and thus to band broadening. On the basis of these considerations, we used a stationary phase packed with 2 μm nonporous particles.

Reversed-phase HPLC separation of IgG2 disulfide isoforms is usually performed at high temperature (65–85 °C) and low pH.<sup>7–11</sup> The use of high temperatures decreases the net affinity of the proteins for the stationary phase by increasing their solubility in the mobile phase, thereby improving their recovery.<sup>10</sup> In our system, increasing the column temperature from 65 to 85 °C increased the peak area (Fig. 2), but did not markedly change the separation performance. Therefore, we used a column temperature of 85 °C, which was the highest temperature we could use in our system. We confirmed that the column could be used 200 times at temperatures higher than 80 °C without obvious performance degradation. Although we used a relatively long column (250 mm) to obtain high resolution,<sup>15</sup> the elution time was almost the same as the elution times reported by researchers who used shorter columns.<sup>10</sup>

We obtained good separation by optimizing the mobile phase gradient; we used the typical gradient of water and

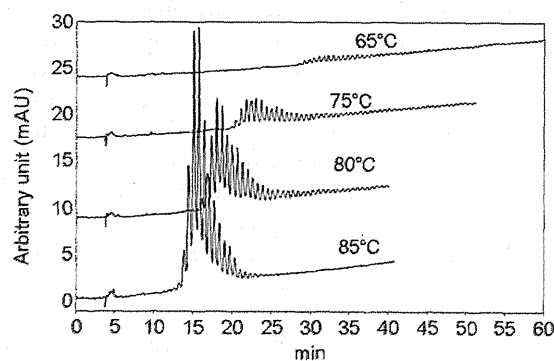


**Fig. 2** Effect of temperature on the chromatographic separation of IgG2#1. Column, Presto FF-C18 (250 × 4.6 mm i.d.); mobile phases: (A) water containing 0.1% trifluoroacetic acid, (B) acetonitrile containing 0.1% trifluoroacetic acid; mobile phase gradient, (B) samples were injected under loading conditions of 34% B, and the proportion of B was increased to 41% B, with a linear elution gradient starting at 0 min and ending at 60 min; flow rate, 400 μL min<sup>-1</sup>; column temperature, 65–85 °C; sample concentration, 2 mg mL<sup>-1</sup>; injection volume, 2 μL.

acetonitrile containing TFA. The chromatograms of two commercially available recombinant monoclonal IgG2s (Fig. 3A) showed many peaks, and the number of separated peaks was more than twice that previously reported (a maximum of four partially separated peaks).<sup>5,7,10,11</sup>

Under optimized conditions, the run-to-run repeatability of the IgG2 separation pattern was satisfactory (data not shown), and the day-to-day repeatability of the retention time of one of the main peaks was also good (relative standard deviation 0.9%). Therefore, the separation pattern of intact IgG can be expected to be useful for monitoring product consistency.

We also analyzed two commercially available IgG1s and one IgG4 under slightly modified separation conditions (the mobile phase gradient was optimized in each case). The chromatograms of IgG1s and IgG4 showed one major peak and a few minor peaks and were similar to chromatograms obtained by previously reported methods.<sup>7,11</sup> These results indicate that our method separated IgG2 isoforms more effectively than the other methods.

To date, three types of disulfide isoforms of IgG2 have been reported. To determine whether our method could separate only disulfide-mediated structural isoforms or whether other variants could be differentiated by our method, we applied it to the IgGs after they had been broken down into their heavy and light chains by reduction with dithiothreitol and subsequently

alkylation with iodoacetic acid. When we analyzed reduced and alkylated IgGs with the same chromatography system, the resulting chromatograms showed two sets of peaks, one set derived from the light chains and the other from the heavy chains (Fig. 4).<sup>10</sup> The light chains showed a single sharp peak, while the peaks derived from the heavy chains of both IgG2s were distributed inhomogeneously (Fig. 4A), and the distribution for the IgG2s differed from the distributions for the IgG1s and IgG4 (Fig. 4B and C). These results indicate that not only heterogeneity in disulfide bonding but also heterogeneity derived from other factors such as the charge or physicochemical properties of the heavy chain might have contributed to the separation obtained by means of our system. The observation of IgG2 charge variants during cation-exchange chromatography has been reported.<sup>10</sup> Further experiments such as mass spectrometry are needed to determine the mechanism by which members of the IgG2 subclass were separated.

In conclusion, the method we developed for HPLC on a column packed with 2  $\mu\text{m}$  nonporous ODS silica particles showed markedly improved separation of recombinant IgG2 isoforms with good repeatability. We suggest that the separation was based in part on recognition of disulfide-based structural isoforms but that other possible separation mechanisms might include heterogeneity in physicochemical properties such as the charge and intermediate of protein refolding. Our

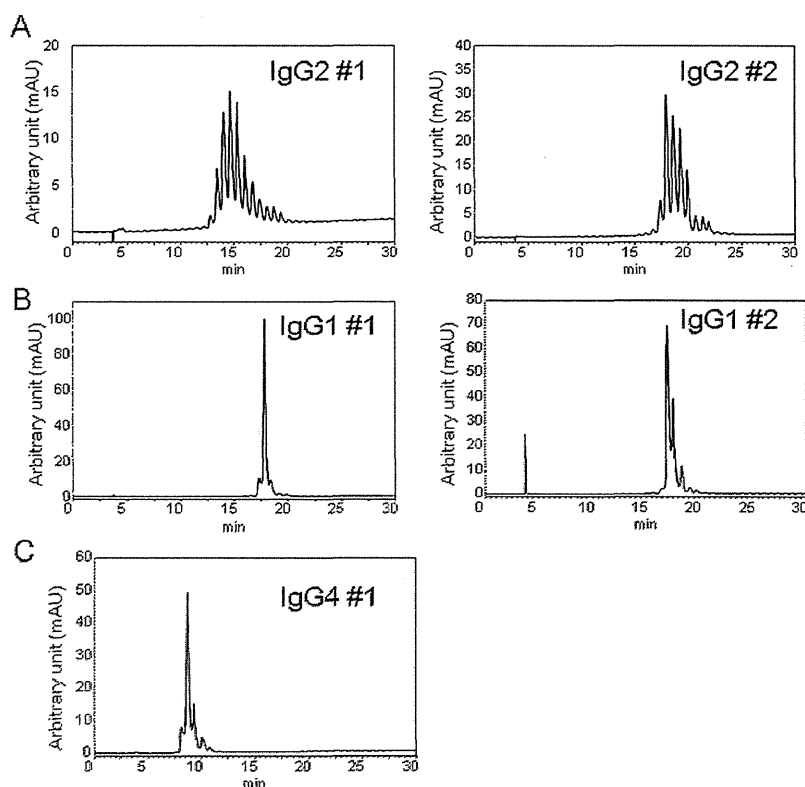


**Fig. 3** Reversed-phase HPLC chromatograms of (A) IgG2s, (B) IgG1s, and (C) IgG4. Mobile phase linear gradients starting at 0 min and ending at 60 min: IgG2#1, 34% (0 min)–41% (60 min), IgG2#2, 32% (0 min)–43% (60 min), IgG1#1 and IgG1#2, 31% (0 min)–44% (60 min), IgG4#1, 33% (0 min)–42% (60 min); column temperature, 85 °C; sample concentration, 1 mg mL<sup>-1</sup>. The other conditions were the same as those described in the legend of Fig. 2.

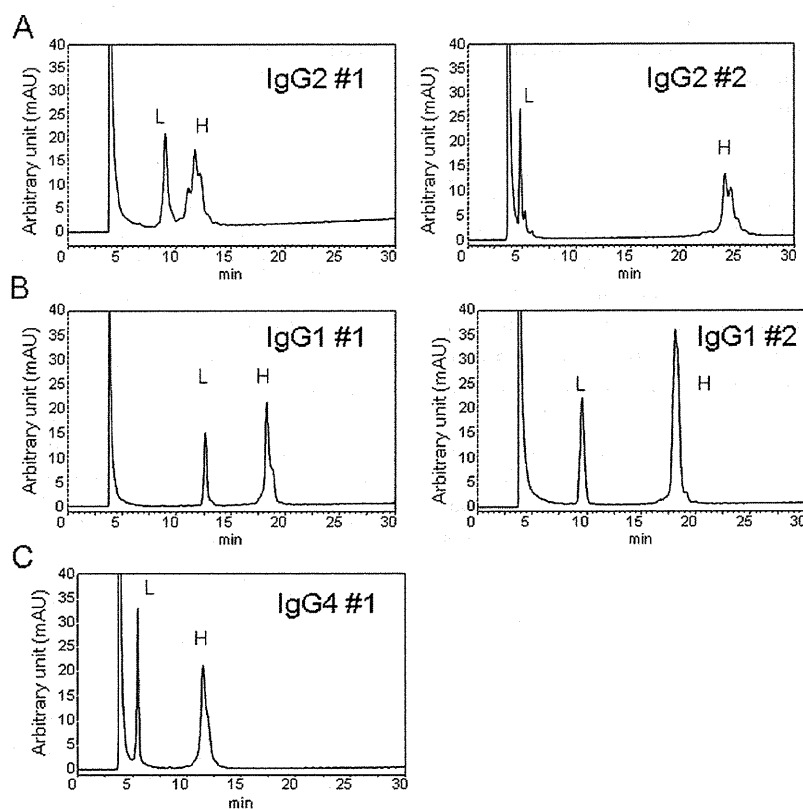


**Fig. 4** Chromatograms of reduced forms of the IgGs whose chromatograms are shown in Fig. 3. The conditions for each IgG were the same as those described in the legend of Fig. 3. L, light chain; H, heavy chain.

method can be expected to be useful for monitoring IgG isoform distributions, which is important for ensuring product consistency during the development and commercialization of therapeutic antibodies.

## Acknowledgements

The authors are grateful for financial support from the Program for Promotion of Fundamental Studies in Health Sciences of the National Institute of Biomedical Innovation (NIBIO) and Health Labor Sciences Research Grant from the Ministry of Health, Labour, and Welfare (MHLW).

## References

- 1 D. O. Beenhouwer, E. M. Yoo, C. W. Lai, M. A. Rocha and S. L. Morrison, *Infect. Immun.*, 2007, **75**, 1424–1435.
- 2 R. Jefferis, *Expert Opin. Biol. Ther.*, 2007, **7**, 1401–1413.
- 3 D. Burton, *Mol. Immunol.*, 1985, **22**, 161–206.
- 4 S. M. Canfield and S. L. Morrison, *J. Exp. Med.*, 1991, **173**, 1483–1491.
- 5 B. Frangione and C. Milstein, *J. Mol. Biol.*, 1968, **33**, 893–906.
- 6 J. Wypych, M. Li, A. Guo, Z. Zhang, T. Martinez, M. J. Allen, S. Fodor, D. N. Kelner, G. C. Flynn, Y. D. Liu, P. V. Bondarenko, M. S. Ricci, T. M. Dillon and A. Balland, *J. Biol. Chem.*, 2008, **283**, 16194–16205.
- 7 T. M. Dillon, M. S. Ricci, C. Vezina, G. C. Flynn, Y. D. Liu, D. S. Rehder, M. Plant, B. Henkle, Y. Li, S. Deechongkit, B. Varnum, J. Wypych, A. Balland and P. V. Bondarenko, *J. Biol. Chem.*, 2008, **283**, 16206–16215.
- 8 Y. D. Liu, X. Chen, J. Z. Enk, M. Plant, T. M. Dillon and G. C. Flynn, *J. Biol. Chem.*, 2008, **283**, 29266–29272.
- 9 T. M. Dillon, P. V. Bondarenko and M. Speed-Ricci, *J. Chromatogr., A*, 2004, **1053**, 299–305.
- 10 T. M. Dillon, P. V. Bondarenko, D. S. Rehder, G. D. Pipes, G. R. Kleemann and M. S. Ricci, *J. Chromatogr., A*, 2006, **1120**, 112–120.
- 11 Q. Wang, N. A. Lacher, B. K. Muralidhara, M. R. Schlittler, S. Aykent and C. W. Demarest, *J. Sep. Sci.*, 2010, **33**, 2671–2680.
- 12 C. Hovarth and H.-J. Lin, *J. Chromatogr.*, 1978, **149**, 43–70.
- 13 N. Wu, Y. Liu and M. L. Lee, *J. Chromatogr., A*, 2006, **1131**, 142–150.
- 14 Imtakt technical information no. T1605E <http://www.imtakt.com/TecInfo/TI605E.pdf>, cited 17 March 2012.
- 15 A. Koshiyama, T. Ichibangase, K. Moriya, K. Koike, I. Yazawa and K. Imai, *J. Chromatogr., A*, 2011, **1218**, 3447–3452.

## 革新的医薬品の開発環境整備を目指したレギュラトリーサイエンス研究

川西徹

## Regulatory science promoting improvement in developing environment of innovative drugs

Toru Kawanishi

Importance of regulatory science in development of innovative drugs is pointed out by the Council for Science and Technology Policy in the Cabinet Office, and the pharmaceuticals-related divisions in the NIHS have begun the regulatory science research for promoting improvement in developing environment of innovative drugs since 2012. Nano-medicines, fully engineered protein drugs, nucleic acid drugs, and gene therapy drugs have been selected as innovative drugs, and the point-to-consider documents for evaluating mainly quality and non-clinical safety of these drugs will be developed. In addition, the conditions for the first-in-human trial will be also proposed, especially from the standpoints of quality and non-clinical safety evaluation.

Keywords: Nano-medicine, Nucleic acid drug, fully engineered protein drug, gene therapy drug

### 1. はじめに —革新的医薬品のレギュラトリーサイエンス (RS) 研究の必要性—

医薬品、医療機器は(1)生命に直接関わる；(2)多くの国で公的医療保険制度により費用負担される公的な性格を有する；(3)それゆえ厳しい規制下にあり、承認基準および市販後においても監視が厳格 という特殊な工業製品である。そのため、近年開発経費の高騰が著しく、新薬の開発が困難になっていることが世界的に指摘されている。一方我が国における医薬品開発環境の問題として、アカデミア等における創業関連の基礎研究レベルは高く医薬品等のシーズは数多く発見されているにもかかわらず、それにみあった日本発の新薬の開発例が少ないこと、さらに医薬品、医療機器の実用化のスピードが欧米に比べて遅く、欧米で承認されていても我国での承認が遅い、いわゆるドラッグラグ、デバイスラグが問題となっている。このような我が国における医薬品の製品化のスピードの遅さの主要な原因の一つとして、製品化及び承認申請・審査の過程のシステム整備が不十分であることが指摘されている。

この状況を打開するために、日本発の医薬品、医療機器、さらに再生医療製品の開発を効率的・効果的に行うためのRS研究を充実・強化し、革新的医療技術の適切な評価、根拠に基づいた審査指針や基準策定等の作成の推進が、“第4期科学技術基本計画（平成23年8月）”および“科学技術イノベーション総合戦略～新次元日本創造への挑戦～（平成25年6月7日）”等において科学技術政策の最重要課題の一つとしてあげられている。

この施策を実現するため、国立医薬品食品衛生研究所では、平成24年度から以下の革新的医薬品、医療機器、および再生医療製品の評価技術開発研究への取り組みを開始している。そこで本稿では、革新的医薬品の評価技術開発研究に絞って、国立衛研における具体的な取組の目的、および成果目標をまとめる。

### 2. 国立医薬品食品衛生研究所における“革新的医薬品の開発環境整備を目指したRS研究”とは

#### (1) 革新的医薬品とは

“第4期科学技術基本計画”あるいは“科学技術イノベーション総合戦略～新次元日本創造への挑戦～”において、「革新的医療技術の研究開発・実用化の推進及び評価手法の確立」が対象とする国立衛研がかかわる「革新的医療技術」としては、まず再生医療製品あるいは医療機器があげられるだろう。それでは、国立衛研が関わる革新的医薬品については、どのような医薬品が対象と

To whom correspondence should be addressed to  
Toru Kawanishi; Director of National Institute of Health Sciences, 1-18-1 Kamiyoga, Setagaya-ku, Tokyo 158-8501, Japan; Tel: +81-3-3700-1141 ext. 200; Fax: +81-3-3700-1340; E-mail: kawanish@nihs.go.jp